附 件 3

PAWEES 2012 International Conference
Challenges of Water & Environmental Management in Monsoon Asia
27-29 November 2012, Thailand

Coping with uncertainties in climate change by stochastic storm rainfall simulation

Ke-Sheng Cheng, Yii-Chen Wu, Yuan-Fong Su, Jun-Jih Liou

Abstract Global warming has had profound impacts on climate and weather of all scales. In coping with such changes, proactive adaptation measures are being sought after. However, planning for adaptation measures requires improved knowledge and quantitative analysis of the uncertainties in climate change. In this study we firstly assessed the effects of climate change on storm rainfall characteristics in Taiwan using the MRI high resolution outputs. Quantitative analysis on changes in storm characteristics of various storm types was also conducted. A stochastic storm rainfall simulation model (SSRSM) which takes into account the physical storm characteristic was developed. The SSRSM is composed of three major components – (1) storm occurrence simulation, (2) (duration, event-total depth) joint simulation, and (3) hyetograph simulation. By setting storm characteristics representative of the projective period, the SSRSM can generate outputs of huge number of simulation runs. Each run yields one annual sequence of hourly rainfalls. From the SSRSM outputs, annual maximum rainfall series of various design durations were extracted and design storm depths of various return periods and durations were obtained through frequency analysis. The SSRSM model has been successfully applied to several regions in Taiwan and details of its application are demonstrated in this paper.

Keywords Climate change, design storm, stochastic simulation, downscaling, uncertainties.

Ke-Sheng Cheng (✉)
Professor
Department of Bioenvironmental Systems Engineering, National Taiwan University
Email: rslab@ntu.edu.tw, Tel: +886-2-33663465, Fax: +886-23635854

Yii-Chen Wu
Postdoctoral Associate
Department of Bioenvironmental Systems Engineering, National Taiwan University
Email: d95622004@ntu.edu.tw

Yuan-Fong Su and Jun-Jih Liou
National Science and Technology Center for Disaster Reduction, Taipei, Taiwan, ROC

Introduction

Many studies related to climate change focus on assessing the climate change effect on earth surface processes in global, continental or regional scale in space and annual, seasonal or monthly scale in time. Climate change effects in local and daily (or hourly) scales, such as the effects on characteristics of rainfall events have received much less attention, possibly due to less and incomplete observed data. However, for practical planning and engineering design, it is necessary to deal with local (spatial) and event (temporal) scales. Moreover, properties of storm events (for example, duration, total depth, peak rainfall rate, etc.) exhibit high degree of variations which are random in nature, and can be characterized as random variables (Koutsoyiannis and Mamassis 2001; Restrepo-Posada and Eagleson 1982). Some of these variables are mutually dependent and have different probability distributions. As a result, it is generally difficult to derive their joint distribution. The complexity of such multivariate variations makes it very difficult to assess the effect of changes in certain variables through multivariate conditional density. An alternative to alleviate such difficulties is by adopting the stochastic simulation approach (Rulli and Rosso 2002; Cameron et al. 2000). Thus, the objective of this study is to develop a continuous storm rainfall simulation model which is capable of characterizing the random nature of storm rainfalls and, through stochastic simulation under certain climate change scenarios, can be used for assessment of the impact of climate change on design storm depth.

Methodology of stochastic storm rainfall simulation

A continuous storm rainfall process can be decomposed into a series of storm events. These storm events are considered independent and the time intervals between the occurrences of two consecutive events are random in nature. Each storm event can then be further characterized by three major factors – the event-total depth, duration, and time distribution of the total depth. All these factors involve high degree of randomness. In light of such complicity, a stochastic storm rainfall simulation model (SSRSM) is desired to tackle the aforementioned random characteristics of storm rainfall process.

Discrete storm occurrences simulation

The annual counts of storms and their time of occurrences are random in nature and can be characterized by two independent random variables. For rare events such as typhoons, their annual counts can be modeled by a Poisson distribution and the time span

between two consecutive typhoons follows an exponential distribution.

Bivariate simulation of the total depth and duration

Generally speaking, the total depth and duration of storm events are correlated. Storms of longer duration tend to produce larger amount of total rainfall depth. Therefore, joint distribution of total depth and duration must be considered in simulation of storm duration and total depth. Depending on storm types (for examples, typhoons, convective storms, and Mei-Yu in early spring), the joint distribution of event-total rainfall and duration can take different forms. In our study, we have found that a bivariate gamma distribution can be used to characterize the (total-depth~duration) joint distribution of typhoon events.

Suppose that random variables X and Y form a bivariate gamma distribution, there exists a corresponding pair of random variables U and V which form a bivariate standard normal distribution. Cheng et al. (2011) proved that the correlation of X and Y (ρ_{XY}) and the correlation coefficient of U and V (ρ_{UV}) has the following single-value relationship:

$$\rho_{XY} \approx (A_X A_Y - 3A_X C_Y - 3C_X A_Y + 9C_X C_Y)\rho_{UV} + 2B_X B_Y \rho_{UV}^2 + 6C_X C_Y \rho_{UV}^3 \quad (1)$$

where γ_X and γ_Y are respectively skewness of X and Y and

$$A_X = 1 + \left(\frac{\gamma_X}{6}\right)^4,\ B_X = \frac{\gamma_X}{6} - \left(\frac{\gamma_X}{6}\right)^3,\ C_X = \frac{1}{3}\left(\frac{\gamma_X}{6}\right)^2,\ A_Y = 1 + \left(\frac{\gamma_Y}{6}\right)^4,$$

$$B_Y = \frac{\gamma_Y}{6} - \left(\frac{\gamma_Y}{6}\right)^3,\ C_Y = \frac{1}{3}\left(\frac{\gamma_Y}{6}\right)^2.$$

The values a random variable can assume can be represented as a function of its frequency factor K:

$$X = \mu_X + K\sigma_X \quad (2)$$

In addition, the frequency factor of a gamma distribution can be expressed by the following equation:

$$K \approx z + (z^2 - 1)\frac{\gamma}{6} + \frac{1}{3}(z^3 - 6z)\left(\frac{\gamma}{6}\right)^2 - (z^2 - 1)\left(\frac{\gamma}{6}\right)^3 + z\left(\frac{\gamma}{6}\right)^4 - \frac{1}{3}\left(\frac{\gamma}{6}\right)^5 \quad (3)$$

Cheng et al. (2011) developed a frequency-factor based approach of bivariate gamma simulation. Given ρ_{XY}, the approach firstly find the corresponding ρ_{UV}, and then a random sample of the bivariate standard normal distribution can be generated. Finally, a random sample of the bivariate gamma distribution is obtained using Equations (2) and (3).

Disaggregation of event-total depth

Incremental rainfall (e.g. hourly rainfall) varies within the duration of a storm event, and thus total rainfall depth of individual storm events must be disaggregated over storm durations. Based on the simple scaling property of incremental rainfall, Cheng et al. (2001) developed a dimensionless hyetograph model. The model disaggregates total depth of a storm event into a fixed number of incremental rainfall depths. Since storm duration varies with events, the time increment of incremental rainfall also varies with events. However, the corresponding scaled dimensionless incremental rainfalls (i.e., incremental rainfall percentages) of different storm events are identically distributed.

Let $\{Y(i),\ i=1,\ldots,n\}$ be the scaled dimensionless incremental rainfalls of a storm event. We consider the time variation of $Y(i)$ as a nonstationary truncated gamma-Markov process. The expected value μ_i, standard deviation σ_i and truncated threshold $y_c(i)$, and the lag-one correlation $\rho(i)$ of $Y(i)$ and $Y(i\text{-}1)$ all can be estimated from observed rainfalls. The Markov property provides a convenient way of simulating the gamma-Markov process through sequential bivariate gamma simulation. Thus, disaggregation of the event-total depth can be achieved by the following procedures:

(1) Generating $y(1)$ by simulation of a gamma density with given mean and standard deviation.
(2) Generating subsequent $y(i)$, $i=2,\ldots,n$ by bivariate truncated gamma simulation.
(3) The scaled dimensionless incremental rainfalls are then multiplied by the event-total depth to yield incremental rainfall depths.

Scenarios setting for SSRSM under climate change

Using outputs from GCM models for the baseline period (1980-1999) and projection period (2020-2039) at grids near several rainfall stations in Taiwan, changes in mean values of storm characteristics such as duration, event-total depth and number of storm events were determined for individual rainfall stations. Table 1 lists storm characteristics of the baseline period at the Taipei station. Table 2 shows changes in storm characteristics at Taipei station Taiwan under climate change (A1B scenario).

Table 1. Storm characteristics at Taipei station (Besaline period: 1980 - 1999)

Storm types	Duration (hrs)			Event-total depth(mm)			Inter-arrival time (hrs)		
	Mean	Std dev	Skew	Mean	Std dev	Skew	Mean	Std dev	Skew
Frontal rainfalls	8.08	6.96	2.03	27.81	25.82	2.88	252.28	393.32	3.25
Mei-Yu	9.85	7.48	2.59	37.91	37.85	2.38	110.04	131.78	2.48
Convective storms	6.37	2.35	0.84	38.17	29.93	2.1	227.88	252.77	1.49
Typhoons	32.41	18.1	0.87	145.02	92.08	1.62	402.88	355.85	1.41

Table 2. Ratio of storm characteristics at Taipei station (besaline period / projection period).

Storm types	Duration (hrs)			Event-total depth(mm)			Inter-arrival time (hrs)		
	Mean	Std dev	Skew	Mean	Std dev	Skew	Mean	Std dev	Skew
Frontal rainfalls	0.96	0.77	0.64	0.94	0.99	1.76	1.10	1.19	0.95
Mei-Yu	1.02	1.36	2.33	1.07	1.31	1.56	1.24	1.22	0.76
Convective storms	1.00	0.96	0.64	0.96	1.00	0.99	1.00	1.01	1.15
Typhoons	0.98	0.79	0.80	0.90	0.64	0.96	1.04	0.92	1.39

Using the frequency-factor based bivariate simulation technique and the disaggregation procedures described earlier, we simulated 500 runs of stochastic storm rainfall simulation under the scenario setting shown in Table 2. The simulations were conducted considering

occurrences of different storm types in different seasons. Each run yields an annual sequence of hourly rainfalls. Two examples of annual sequence of hourly rainfalls are shown in Figure 1.

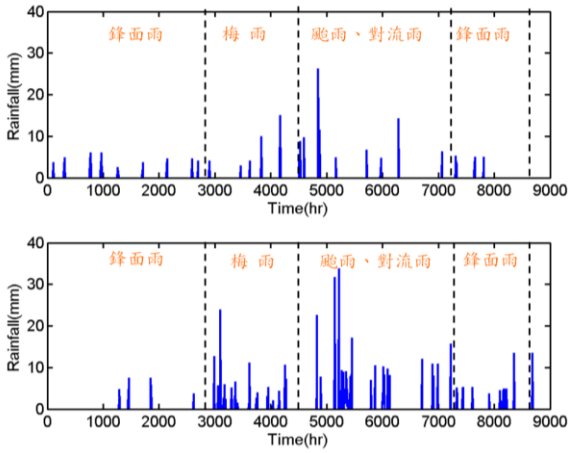

Figure 1. Two simulated annual sequences of hourly rainfalls.

Frequency analysis of simulated rainfalls

From the simulated hourly rainfall data, annual maximum rainfalls of selected design durations were extracted. The annual maximum rainfalls are considered having Pearson type III distributions and design storm depths of 10, 20, 50, 100 and 200-year return periods were calculated. Tables 3 and 4 list the design storm depths of the baseline and projection periods at Taipei station.

Table 3. Design storm depths (in mm) at Taipei station. (Baseline period)

Duration (hours)	Return period (years)				
	10	20	50	100	200
24	296.0	357.2	437.8	498.7	559.5
48	347.9	410.0	489.8	549.1	607.6
72	374.2	425.5	488.0	532.5	575.3

Table 4. Design storm depths (in mm) at Taipei station. (Projection period)

Duration (hours)	Return period (years)				
	10	20	50	100	200
24	307.8	374.5	462.4	528.6	594.5
48	356.4	421.4	503.5	563.2	621.0
72	381.1	433.2	494.6	536.6	575.5

Assessing the effect of climate change on design storm depth

From the results of frequency analysis, it can be found that even though the event-total depths and annual counts of typhoons are likely to reduce in the projection period, rainfall depths of 24-hour design duration will increase by approximately 4% to 6% for return periods ranging from 10 to 200 years. Such increases can be attributed to shorter durations of major storms under climate change. It also suggests that the area will experience storms with higher rainfall intensities in the projection period.

Conclusions

A few concluding remarks from the preliminary results are drawn below:

(1) The stochastic storm rainfall simulation model provides a means for assessing the impact of climate change on design storm depths.

(2) Under the given scenario setting, design storm depths of 24 to 72 hours durations and 10 to 200 return periods are likely to increase in the projection period. Such increases can be attributed to shorter durations of major storms under climate change. It also suggests that the area will experience storms with higher rainfall intensities in the projection period.

Acknowledgments

This work has been partly supported by the National Science Council, Water Resources Agency and the Council of Agriculture of Taiwan. We are also grateful to NCDR TCCIP teams for providing GCM outputs and technical supports.

References

Cameron D, Beven K, Tawn J (2000) An evaluation of three stochastic rainfall models. Journal of Hydrology 228, 130–149.

Cheng KS, Hueter I, Hsu EC, Yeh HC (2001) A scale-invariant Gauss-Markov model for design storm hyetographs. Journal of the American Water Resources Association, Vol. 37, No. 3, 723-736.

Cheng KS, Hou JC, Liou JJ (2011) Stochastic simulation of bivariate gamma distribution – A frequency-factor based approach. Stochastic Environmental Research and Risk Assessment, 25(2): 107 – 122, DOI 10.1007/s00477-010-0427-7.

Koutsoyiannis D, Mamassis N (2001) On the representation of hyetograph characteristics by stochastic rainfall models. Journal of Hydrology, 251, 65 – 87.

Restrepo-Posada PJ, Eagleson PS (1982) Identification of independent rainstorms. Journal of Hydrology, 55, 303-319.

Rulli MC, Rosso R (2002) An integrated simulation method for flash-flood risk assessment. Hydrology and Earth System Sciences, Vol. 6, No. 2, 267-283.

PAWEES 2012 International Conference
Challenges of Water & Environmental Management in Monsoon Asia
27-29 November 2012, Thailand

Investigating the interactive recharge mechanisms between surface water and groundwater over the Jhuoshuei River Basin in Central Taiwan

Fi-John Chang*, Kuang-Chih Chang, Cheng-Hsien Lin, Kuo-Wei Wang, Yu-Hsuan Kao, Li-Chiu Chang

Abstract In Taiwan, groundwater becomes important in dry periods or areas lack of water storage facility due to its low cost, steady water supply and good water quality. However improper groundwater development brings about serious decreases in groundwater levels and land subsidence so that causes disasters, such as seawater intrusion or soil salination, accompanied with environmental and economical losses. It is critical to develop strategies for water resources conservation in mountainous areas. This study aims to investigate the interactive mechanisms of groundwater recharge at the mountainous areas of the Jhuoshuei River basin in Central Taiwan through analyzing and modeling the groundwater level variations. Several issues are discussed in this study, which includes the correlation between groundwater level variation and rainfall as well as streamflow, the identification of groundwater recharge patterns, and effective rainfall thresholds for estimating groundwater level variations. The results indicate: 1) the daily variation of groundwater level is closely correlated with river flow and one-day antecedent rainfall based on correlation analyses; 2) effective rainfall thresholds can be identified successfully;3)groundwater level variations can be classified into four types for monitoring wells; and 4) the daily variations of groundwater level can be well estimated by constructed artificial neural networks.

Keywords Rainfall, Streamflow, Groundwater Level, Artificial Neural Network (ANN), Thiessen polygons method.

Fi-John Chang(✉) · Cheng-Hsien Lin · Kuo-Wei Wang · Yu-Hsuan Kao
Professor
Dept. of Bioenvironmental Systems Engineering, National Taiwan University, No. 1, Sec. 4, Roosevelt Road, Taipei 10617, Taiwan, ROC.
E-mail: changfj@ntu.edu.tw
Tel: +886-2-33663452; Fax: +886-2-23635854

Kuang-Chih Chang
Water Resources Agency, Ministry of Economic Affairs, Taipei 10651, Taiwan, ROC

Li-Chiu Chang
Department of Water Resources and Environmental Engineering, Tamkang University, New Taipei City 25137, Taiwan, ROC

Introduction

In the last decades, water demand has increased drastically due to the rapid development in economy and industry in Taiwan. Because of the uneven spatial and temporal distribution of rainfall and insufficient water storage facilities, groundwater has become an important water source for agricultural, industrial and domestic water users during drought periods and/or at the areas short of water storage facilities through considering several features of groundwater such as low-cost, stable water temperature, constant water quantity, good water quality and easy accessibility. However, due to inappropriate industrial and/or environmental development, groundwater levels drop seriously at some coastal areas in Taiwan, and the subsidence phenomenon, seawater intrusion, soil salinization and seawater intrusion results in disasters that cause a dual loss in environment and economy. Groundwater level variations can be affected by various factors such as human extraction or injection, earth tides, atmospheric pressure changes, temperature and rainfall. Groundwater level variations observed by groundwater level monitoring wells are rather comprehensive, which includes the variation trend of natural dissipation of groundwater levels, the causes of water level variations induced by atmospheric pressures, earth tides, rainfall and earthquake, and other factors (Bredehoeft 1967; Jacob 1940; Matsumoto 1992; Rojstaczer 1988; Van der Kamp and Gale 1983). Cheng et al. (2003) applied the time series to analyzing the relationship between rainfall and groundwater level and showed that rainfall can be regarded as a leading indicator of groundwater level. The finding of Chen et al. (2005) indicated that the time lag between rainfall and groundwater level variation might occur. Chen (2006) found that groundwater level is affected by rainfall with different response time, where the rapid response time may be within a few hours while the slow response time may take few days, and different initial soil water contents also make certain impacts on lag time.

Artificial neural networks (ANNs) are a learning and computing technology that mimics biological neural systems, where the network constructs a neural system with receipt and response abilities through continually absorbing previous experiences and performing iterative

computation by using computers. With advanced development in technology and powerful computation ability of computers, ANNs have been widely used in various disciplines and fields (Mamdani and Assilian 1975; Memdel 2001; Nayak et al. 2004;Nourani et al. 2008;Chen and Chang 2009; Nouraniet al. 2011; Chang et al. 2010; Chang et al. 2012). Daliakopoulos et al. (2005) used seven different ANN structures to predict the groundwater level of monitoring wells on Crete island of Greece through, and the results demonstrated that it is sufficient to use monthly models for predicting yearly groundwater levels. Nayak (2006) applied the ANN to forecasting thegroundwater level of India's coastal plain and indicated that the ANN can precisely and appropriately forecast groundwater levels in the next few months with a forecast error of about 35 cm.

Understanding the interactive recharge mechanism between mountainous water resources and groundwater can facilitate future discussion on mountainous water resource conservation strategy for alleviating land subsidence in downstream areas. So far, few studies have discussed about the groundwater recharge mechanism at mountainous area. To investigate the groundwater level variations at the mountainous areas, the Jhuoshuei River basin of the Central Taiwan is used as a case study.

Methodology

This study aims to investigate the interactive recharge mechanisms between surface water and groundwater over the Jhuoshuei River basin in Central Taiwan by using an artificial neural network coupled with statistical analyses. The methodology used consists of the Pearson correlation coefficient, the Thiessen polygons method and the back-propagation neural network, which are briefly addressed as follows:

Pearson Correlation Coefficient

In this study, the Pearson correlation coefficient (Pearson 1896) is used to identify the time lags between groundwater level variations and rainfall as well as streamflow. The Pearson correlation coefficient, or "Pearson product-moment correlation coefficient", is a quantitative method that measures the dependence between two quantities, which can be obtained by dividing the covariance of the two variables by the product of their standard deviations.

The Pearson correlation coefficient ranges from −1 to 1. A value of 1 indicates a positive (increasing) perfect linear relationship, a value of −1 indicates a negative (decreasing) perfect linear relationship, and a value of 0 indicates no linear relationship (uncorrelated) is detected. The closer the coefficient is to either −1 or 1, the stronger the correlation between two variables is. For a series of n variables of X and Y (denoted by x_i and y_i, respectively, where $i = 1,2,\ldots, n$), the sample correlation coefficient can be used to estimate the population Pearson correlation r between X and Y. The sample correlation coefficient is given as:

$$r_{xy} = \frac{\sum_{i=1}^{n}(x_i-\bar{x})(y_i-\bar{y})}{(n-1)s_x s_y} = \frac{\sum_{i=1}^{n}(x_i-\bar{x})(y_i-\bar{y})}{\sqrt{\sum_{i=1}^{n}(x_i-\bar{x})^2\sum_{i=1}^{n}(y_i-\bar{y})^2}} \quad (1)$$

where x and y are the sample means of X and Y accordingly, and s_x and s_y are the sample standard deviations of X and Y accordingly.

Thiessen Polygon Method

The Thiessen polygon method was developed by Thiessen (1911), which is a method used to approximate the relative significance of data from points scattered arbitrarily across an area. The Thiessen polygon method introduces the concept of weighting, compared with the arithmetic averaging method. Therefore, the Thiessen polygon method is very useful when calculating rainfall in a given area. Thiessen polygons can be constructed by intersecting the perpendicular bisector lines between each pair of points. The formula of the Thiessen polygon method used in this study is shown as follows:

$$\bar{p} = \frac{\sum_{i=1}^{N} P_i A_i}{\sum_{i=1}^{N} A_i} \quad (2)$$

where $\bar{p}$ is the average rainfall (mm) of the area, N is the number of rainfall gauging stations of the area, P_i is the rainfall of the i^{th} rainfall gauging station of the area, and A_i is the controlling area (m^2)

Back-Propagation Neural Network (BPNN)

In this study, the BPNN is used to construct estimation models for groundwater level variations owing to its superior nonlinear mapping ability.

The BPNN, developed by Rumelhart et al. (1986), is the most prevalent network among the supervised learning networks in ANNs. The BPNN uses the gradient steepest descent method to modify the weights of interconnected neurons and easily manages the interactions of processing elements by adding hidden layers. In the learning process, the interconnection weights are adjusted by using an error convergence technique to obtain the desired output for a given input. In general, the error of the output layer will propagate backward to the input layer through hidden layers to obtain the desired output in the BPNN model. The gradient descent method is utilized not only to calculate the weight of the network and but to adjust the weight of interconnections so that minimize the output error. The structure of the BPNN model is shown in Fig. 1, and the formula is given below.

In the BPNN, the input of the j^{th} neuron of the n^{th} hidden layer is the nonlinear function of the output of the $(n-1)^{th}$ hidden layer.

$$y^n{}_j = F(net^n{}_j) \quad (3)$$

where y^n_j is the output of the n^{th} hidden layer, F is the activation function, and $net^{\ n}_j$is the summation of weighted input X_i of the $(n\text{-}1)^{th}$ hidden layer, which is shown below:

$$net_j = \sum_{i=1}^{m} w_{ji} x_i + b_j \quad (4)$$

where w^n_{ji} is the connection weight of the j^{th} neuron in the n^{th} hidden layer and the i^{th} neuron in the $(n\text{-}1)^{th}$ hidden layer, and b^n_j is the bias of the j^{th} neuron in the n^{th} hidden layer.

Because the BPNN isa supervised learning network, it aims to reduce the difference between network outputs and target outputs. The error function E is defined as:

$$E = \frac{1}{2}\sum_k (d_k - y_k)^2 \quad (5)$$

where d_k is the target output of the k^{th} neuron, and y_k is the network output of the k^{th} neuron.

In general, the connection weights of the BPNN could be easily obtained by using the abovementioned algorithm, and the applicability of the constructed network should be further validated and tested. Consequently, data sets are commonly distributed into three independent sets for training, validating and testing, respectively, for the purpose of network configuration, validation and testing. The network would be trained to obtain their optimized connection weights based on the input-output patterns in the training data set, select the most suitable constructed network by using the validating data set, and then be further tested the applicability and reliability of the selected network by using the testing set.

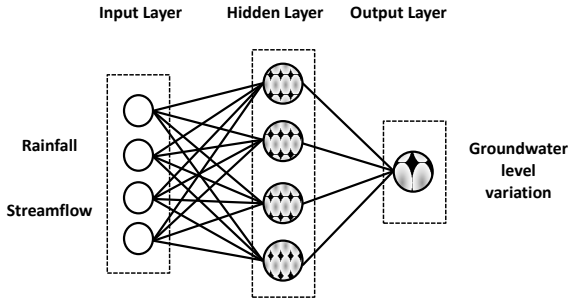

Fig.1. Structure of the BPNN model

Case Study

This study aims to investigate the groundwater recharge mechanism at mountainous area in the Jhuoshuei River basin through analyzing the groundwater level variations. The Jhuoshuei River with a total length of 186.6 km is the longest river in Taiwan, and its drainage area is about 3156 square kilometers, which is the second largest drainage area in Taiwan. The Jhuoshuei River basin is located in Central Taiwan and has the highest elevation of about 3,200 meters. Its topographical terrain decreases from east to west (i.e. with terrain slope increases from west to east). Due to the highly complex topographical terrain of the Jhuoshuei River basin, rainfall is unevenly distributed and is concentrated in a five-month period starting from May to September. The total rainfall in the wet period accounts for 75% of the total annual rainfall, which implies there is a big difference of rainfall between wet and dry periods.

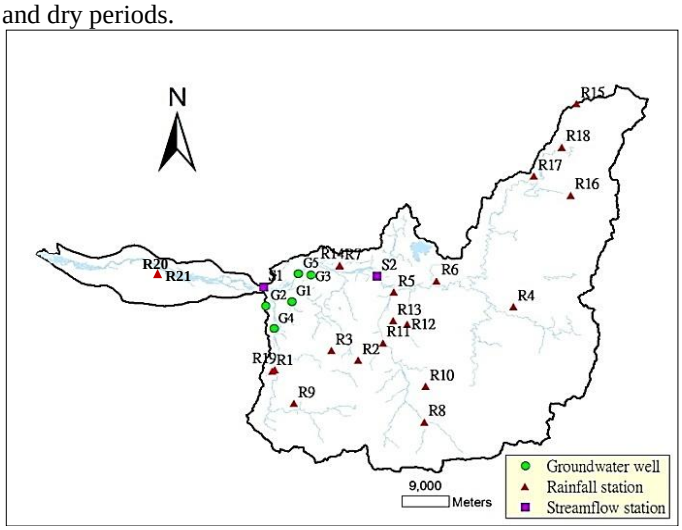

Fig. 2. Distribution of streamflow gauging stations, rainfall gauging stations and groundwater level monitoring wells

In the study area, groundwater level monitoring wells were built over the pass, and streamflow and rainfall gauging stations are located at the midstream and upstream of the Jhuoshuei River (Fig. 2). Data of groundwater level, streamflow and rainfall in the Jhuoshuei River basin are rather complete. Groundwater level and streamflow data were collected from the Water Resources Agency, Taiwan, while rainfall data were collected from the Water Resources Agency, Central Weather Bureau and Taiwan Power Company, Taiwan. The collection period of daily data ranged from 2001 to 2010 in a total of eighteen rainfall gauging stations, four streamflow gauging stations and eight groundwater level monitoring wells (Tables 1-3). Missing data were infilled by using linear regression techniques based on the data of surrounding stations. The flowchart of the groundwater recharge mechanism is shown in Fig. 3.

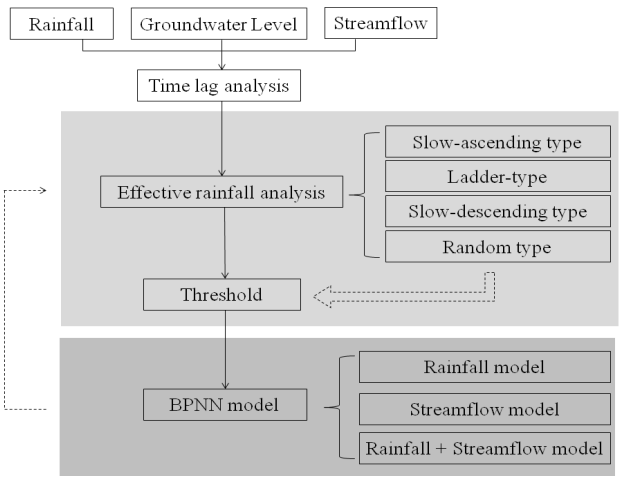

Fig.3. Flow chart of the groundwater recharge mechanism

Table 1 Basic information of eighteen rainfall gauging stations in the study area

Rainfall station	Elevation (m)	X-coordinate (TWD67)	Y-coordinate (TWD67)
R1	400	213782.9	2615639.8
R2	1771	229514.0	2617731.8
R3	1453	224643.7	2619615.9
R4	1700	258098.0	2628024.9
R5	296	236100.2	2630828.7
R6	393	243999.4	2632976.6
R7	203	226228.7	2635948.1
R8	1135	241748.0	2605846.0
R9	724	217736.7	2609447.3
R10	2200	241950.2	2612736.2
R11	485	234079.6	2621048.4
R12	1666	238586.6	2624704.8
R13	322	236038.3	2625353.0
R14	215	226228.9	2636040.4
R15	2303	269710.0	2667105.2
R16	1200	268659.9	2649507.1
R17	890	261871.4	2653191.4
R18	1520	266952.6	2658733.9
R19	231	214240.5	2615918.5
R20	17	193447.9	2633516.6
R21	30	194777.1	2633203.8

Table 2 Basic information of four streamflow gauging stations in the study area

Streamflow station	X-coordinate (TWD67)	Y-coordinate (TWD67)
S1	212103.2	2631755.0
S2	232943.2	2633859.0
S3	234363.9	2634798.0
S4	194978.4	2634095.0

Observation data were divided into the training, validation and testing phases of the BPNN model in the ratio of 6:2:2, respectively, for evaluating the performance of the estimation model. The evaluation criteria for model performance consist of the Pearson correlation coefficient and root mean square error (RMSE) given below:

$$RMSE = \sqrt{\frac{\sum_{t=1}^{N}\left[\hat{Q}(t) - Q(t)\right]^2}{N}} \quad (6)$$

where $\hat{Q}$ is the estimated value and Q is the observed value, and N is the number of data.

The RMSE is used to observe the estimation accuracy of the groundwater level variations. The lower the RMSE value is, the better the model performance is.

Result and Discussion

Time delay analysis

This study adopts the Pearson correlation coefficient to analyze the daily time-delay relationship between groundwater level variation and rainfall through investigating current groundwater level variation versus rainfall of the current day up to the previous nine days. A higher value of the Pearson correlation coefficient indicates a stronger relationship between groundwater level variation and rainfall. Figure 4 shows the results of the Pearson correlation coefficient analysis on groundwater level variations versus rainfall of different time lags at groundwater level monitoring wells. The results indicate that the patterns of groundwater level variations versus rainfall of different time lags are similar, and the highest correlation occurs on the previous day prior to current day for rainfall. Therefore, rainfall on the previous day prior to current day【R(t-1)】is determined as an input to the BPNN model for estimating groundwater level variations.

Similarly, the Pearson correlation coefficient is used to detect the daily time-delay relationship between groundwater level variation and streamflow. The results are illustrated in Fig. 5, which also indicates the patterns of groundwater level variations versus streamflow are similar at each monitoring well, and the highest correlation occurs on the current day for streamflow. Therefore, streamflow on the current day is determined as an input to the BPNN model for estimating groundwater level variations.

Table 4 Weights of rainfall gauging stations for the Thiessen polygon method in the study area

Station	Weight	Station	Weight
R1	0.0064	R12	0.0263
R2	0.0328	R13	0.0113
R3	0.0421	R14	0.0178
R4	0.1834	R15	0.0309
R5	0.0314	R16	0.0753
R6	0.0615	R17	0.0420
R7	0.0424	R18	0.0287
R8	0.1090	R19	0.0253
R9	0.0677	R20	0.0486
R10	0.0659	R21	0.0331
R11	0.0182		

Table 3 Basic statistics of eight groundwater level monitoring wells in the study area

Monitoring well	Well depth (m)	X-coordinate (TWD67)	Y-coordinate (TWD67)	Groundwater level (m)				
				Max	Min	Average	SD[1]	Variance
G1(1)	102.6	217282	2629020	146.6	138.5	141.8	1.91	3.65
G1(2)	199.3	217282	2629020	145.4	136.3	142.7	1.53	2.33
G2	204.5	212545	2628234	202.2	189.9	196.0	2.69	7.25
G3	24.1	220800	2634163	176.0	167.5	169.2	1.06	1.12
G4(1)	52.0	213977	2623841	169.1	161.5	166.5	0.75	0.56
G4(2)	102.0	213977	2623841	170.4	164.4	167.5	0.89	0.79
G5(1)	78.2	218500	2634400	145.2	133.0	137.7	2.24	5.00
G5(2)	193.2	218500	2634400	139.5	132.2	135.6	1.50	2.24

[1] Standard deviation

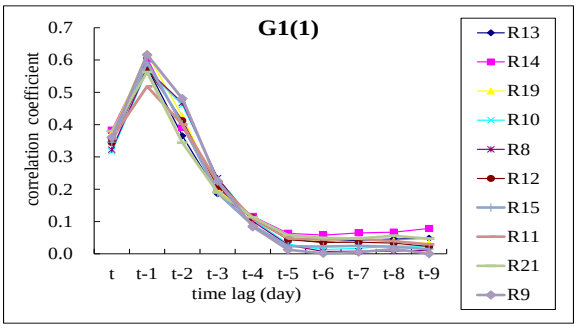

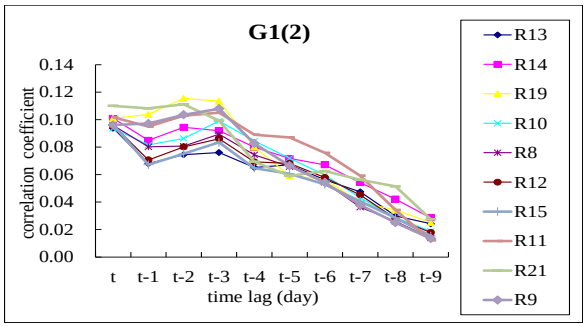

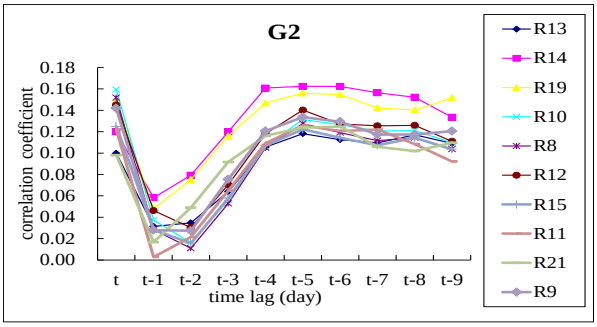

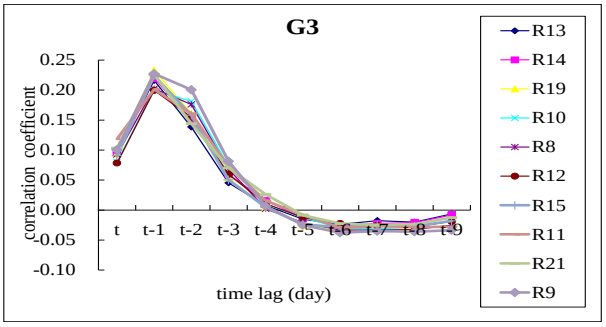

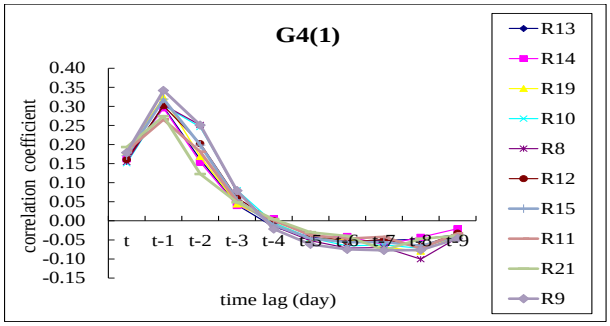

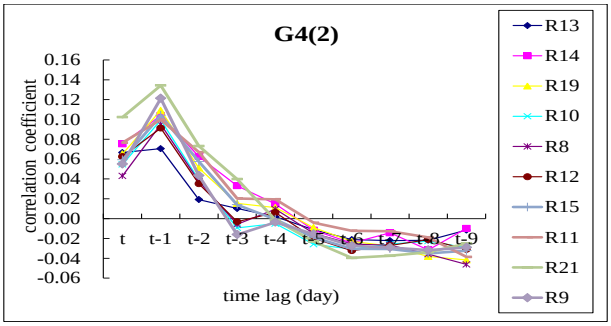

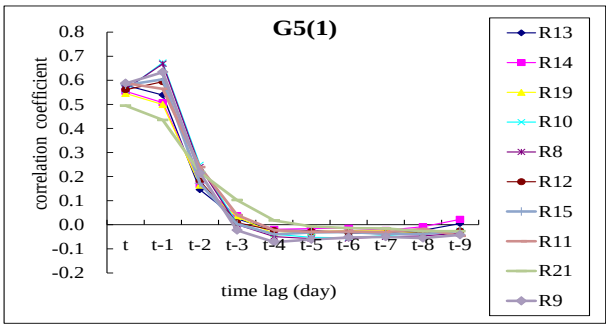

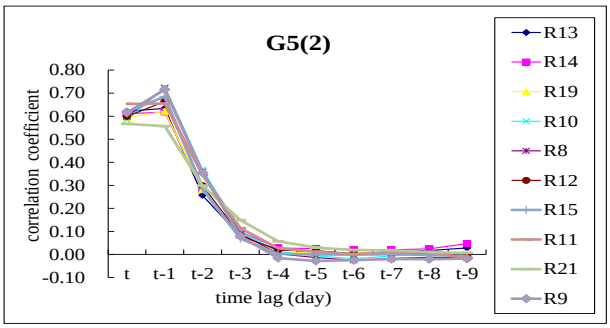

Fig. 4. Correlation between groundwater level variation and rainfall of different time lags at groundwater level monitoring wells

Effective rainfall threshold analysis

According to the data collected in this study, it reveals that variations still occur in groundwater levels when it does not rain, which results in a low correlation between groundwater level variation and rainfall. This study makes an assumption that rainfall over certain threshold can significantly affect groundwater level variations. Therefore this study adopts the Thiessen polygon method to calculate the average rainfalls over the basin area at different thresholds for identifying thresholds. Table 4 shows the weights of rainfall gauging stations for the Thiessen polygon method. A total of 3620 rainfall data were screened at different thresholds ranging from 0 mm to 15 mm with an increment of 1 mm. Consequently, four types of patterns can be clearly classified after correlation analyses between groundwater level variations and rainfall filtered at different thresholds:

Slow-ascending type:

Groundwater monitoring wells G1(1) and G4(2) are classified as the slow-ascending type (Fig. 6(a)). After filtering out rainfall data below the threshold of 2 mm, the correlation between groundwater level variations and rainfall significantly improves and shows an ascending trend. This ascending trend becomes less obvious when rainfall thresholds are higher than 2 mm. The ascending trend might be because the depth of these two wells are around 102 meters (at medium depth) so that it takes longer time for rainfall to infiltrate into these two wells. By filtering out small rainfalls (< 3 mm), the effective rainfall is identified and thus the correlation improves significantly. However, the correlation becomes flatter towards higher rainfall thresholds.

Ladder-type:

Groundwater monitoring wells G3 and G4(1) are classified as the ladder-type. For G4(1), sudden increases in the correlation coefficients occur at rainfall screening thresholds of 1 mm and 7 mm, respectively (Fig. 6(b)). Similarly for G3, sudden increases in the correlation coefficients between groundwater level variations and rainfall occur at rainfall screening thresholds of 1 mm and 5 mm, respectively. The causes of such phenomena might be due to the shallow depths of these two wells (G3: 24.1 meters; G4(1): 52 meters) and the geologic structures of the wells. Apparently, the response to correlation is increasing when rainfall thresholds increase. In particular, the topsoil structure of G4(1) is of the clay layer, the infiltration of rainfall into this well would start only when rainfall reaches a certain degree, and thus the correlation is of a ladder-shape.

Slow-descending type:

Groundwater monitoring wells G5(1) and G5(2) are classified as the slow-descending type (Fig. 6(c)). The correlation between groundwater level variations and rainfall decreases and shows a descending trend when rainfall thresholds increase. The cause of the descending trend might be due to the geological structures of these two wells. The geological structure of these two wells is of the gravel layer, and therefore water mobility becomes fast owing to the high porosity of the gravel layer. In particular, the high water mobility of these two wells makes both wells within the same aquifer even though their well depths are different (G5(1): 78.2 meters; G5(2): 193.2 meters). Rainfall infiltrates very quickly no matter how high the rainfall intensity is, and thus the use of rainfall thresholds would reduce the correlation between groundwater level variations and rainfall. However the correlations of these two wells are about 0.6 without conducting any rainfall screening, despite that both wells belong to the slow-descending type.

Random type:

Groundwater monitoring wells G2 and G1(2) are classified as the random type (Fig. 6(d)). Both G2 and G1(2) have low correlations between groundwater level variations and rainfall. The well depths of G2 and G1(2) are 204.5 m and 199.3 m, respectively (at deep depth), while the infiltration rate of rainfall into groundwater is tens of meters per day. Therefore, the impact of recharge from rainfall to groundwater is comparatively small for deep-depth wells such as G2 and G1(2), which might be the cause for the low correlation between groundwater level variations and rainfall. Besides, the correlation does not increase even though rainfall thresholds increase.

Estimation model of groundwater level variations

This study proposes an estimation model of groundwater level variations by using the BPNN. There are eighteen rainfall gauging stations in total. It will reduce the learning and training efficiency of the BPNN model if data of all eighteen rainfall gauging stations are incorporated as inputs into the model. Therefore, data of rainfall gauging stations that are highly correlated with groundwater level variations are determined as model inputs. Besides, data of streamflow gauging stations S3 and S4 are not considered as inputs to the model because S3 is located near Ming-Tan Reservoir and thus is directly affected by reservoir operations while S4 is located far from groundwater level monitoring wells and thus has less influence on the groundwater level variations of monitoring wells. In Table 5, groundwater level monitoring wells G1(1), G3 and G4(1) have higher correlation coefficients with rainfall than with streamflow, conversely G5(1) has higher correlation coefficients with streamflow than with rainfall. From 2, it shows G5(1) is located right next to the Jhuoshuei river, and thus the groundwater level variation of G5(1) is apparently influenced by the lateral recharge from the river. This condition is consistent with the results that G5 has higher correlation with streamflow than the other three wells.

Table 5 Correlation of model input and output

Output (Monitoring well)	Input (Rainfall)	Corr[1]	Input (Streamflow)	Corr
G1(1)	R1	0.73	S1	0.69
	R7	0.70	S2	0.68
	R9	0.75		
	R14	0.71		
	R19	0.73		
G5(1)	R8	0.77	S1	0.80
	R9	0.75	S2	0.76
	R10	0.75		
G3	R1	0.63	S1	0.55
	R13	0.60	S2	0.60
	R14	0.60		
	R19	0.64		
G4(1)	R1	0.74	S1	0.67
	R9	0.76	S2	0.65
	R19	0.75		

[1] Correlation coefficient

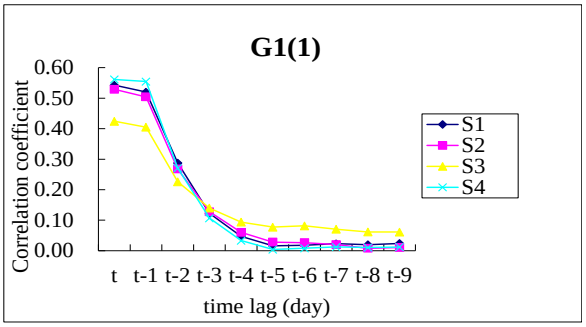

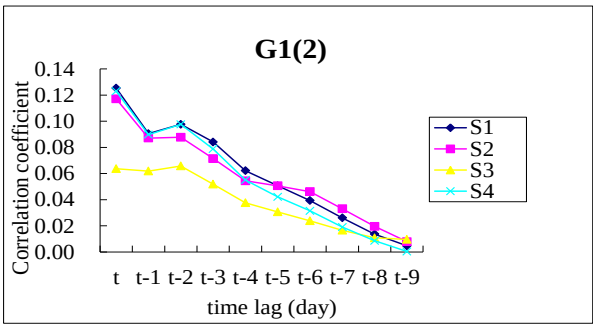

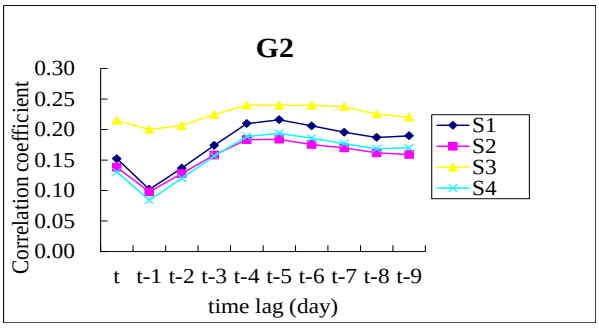

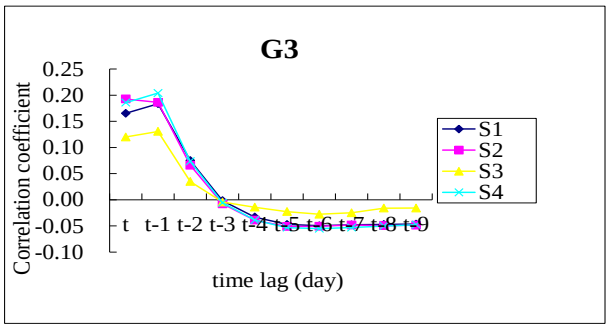

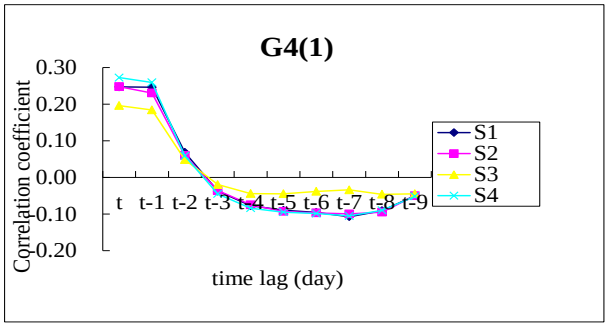

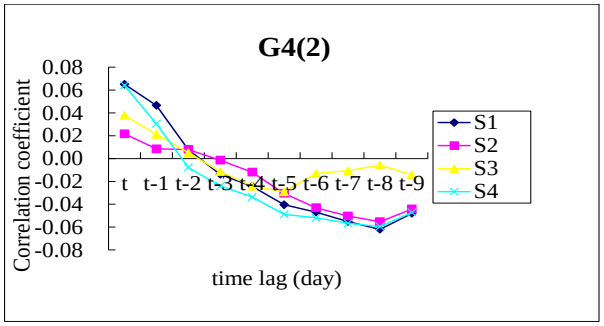

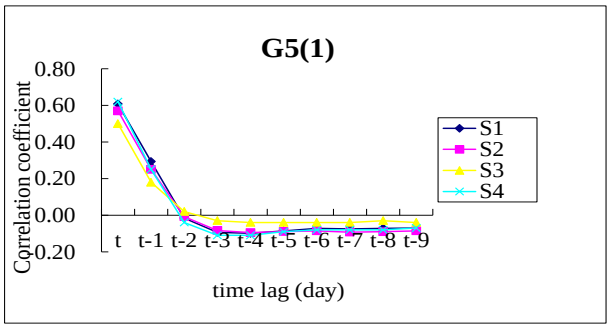

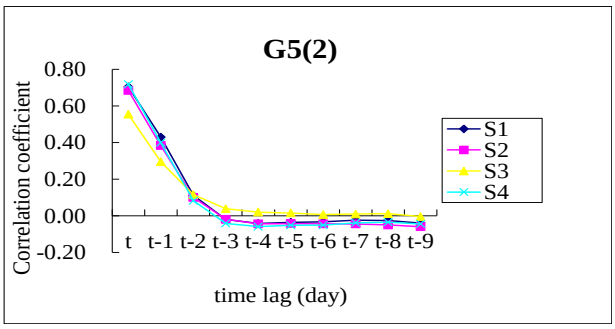

Fig. 5. Correlation between groundwater level variation and streamflow at groundwater level monitoring wells

For the estimation of groundwater level variation, this study investigates five estimation models established with difference input combinations: without thresholding (streamflow, rainfall); and with thresholding (streamflow, rainfall, streamflow+rainfall). Table 6 displays the estimation results of the BPNN models for groundwater level monitoring wells G1(1), G3, G4(1) and G5(1).

G1(1): slow-ascending type

The best structure of the BPNN model for G1(1) has one hidden layer and four neurons. Observation data are divided into the training, validation and testing phases in the ratio of 6:2:2, respectively. The total number of groundwater level variation data for G1(1) is 1306. After conducting the rainfall threshold screening at the effective threshold of 1 mm, only 780 data remain for use. Without conducting the rainfall threshold screening, the correlation coefficient between observed and estimated values is 0.66 in the testing phase for the streamflow model, similarly, the correlation coefficient is 0.71 for the rainfall model. The results of the models with effective thresholds significantly improve model

performance: the correlation coefficient between observed and estimated values increases from 0.66 to 0.71 (improvement rate: 8%) in the testing phase for the streamflow model, similarly, and the correlation coefficient increases from 0.75 to 0.80 (improvement rate: 7%) for the rainfall model. In addition, rainfall models outperform streamflow models in terms of correlation and RMSE values, which coincides with the results of G1(1) in Table 5. The reason might be G1(1) is a little bit far from the Jhuoshuei River and is less influenced by the lateral recharge from the river, and thus streamflow models have less performance than rainfall models. Alternatively, the estimation model combining streamflow and rainfall as inputs performs the best with the correlation coefficient of 0.91 in the testing phase, which indicates both rainfall and streamflow is important information to this estimation model.

G5(1): slow-descending type

The best structure of the BPNN model for G5(1) has one hidden layer and three neurons. Observation data are divided into the training, validation and testing phases in the ratio of 6:2:2, respectively. The total number of groundwater level variation data for G5(1) is 1065. After conducting the rainfall threshold screening at the effective threshold of 0 mm, only 821 data remain for use. However the estimation results indicate that it makes little improvements in the correlation coefficients between data without and with threshold screening for streamflow models (0.86 to 0.87 in the testing phases) and rainfall models (0.77 to 0.81 in the testing phases). In addition, streamflow models outperform rainfall models, which also coincides with the results of G5(1) in Table 5. This is because G5(1) is located right next to the Jhuoshuei river and is significantly affected by the lateral recharge from the river. Alternatively, the estimation model combining streamflow and rainfall as inputs performs the best with the correlation coefficient of 0.89in the testing phase, which implies streamflow significantly affects groundwater level variation in this well even though conducting rainfall threshold screening does not make a big improvement in the estimation results of the rainfall model.

G3: ladder-type

The best structure of the BPNN model for G3 has one hidden layer and five neurons. Observation data are also divided into the training, validation and testing phases in the ratio of 6:2:2, respectively. The total number of groundwater level variation data for G3 is 1203. After conducting the rainfall threshold screening at the effective threshold of 5 mm (the 2nd sudden increase in correlation coefficients), only 370 data remain for use. The estimation results indicate that conducting rainfall threshold screening also makes excellent improvements in the correlation values for streamflow models (0.25 to 0.62, 148% improvement in the testing phases) and rainfall models (0.43 to 0.82, 91% improvement in the testing phases). Similar results are shown in RMSE values. In addition, rainfall models outperform streamflow models, which also coincides with the results of G3 in Table 5. This might be because G3 is located a little bit far from the Jhuoshuei River, and thus

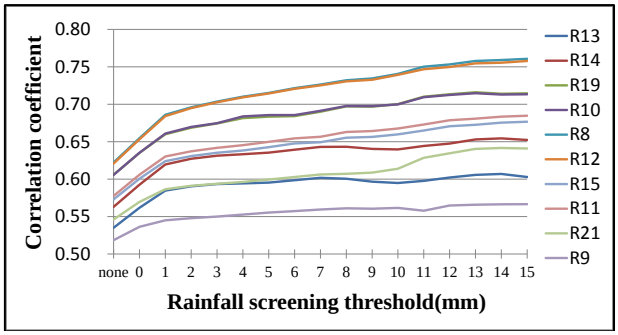

(a) G1(1): slow-ascending type

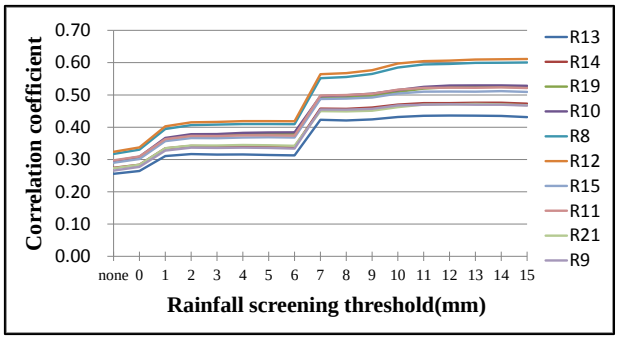

(b) G4(1): ladder-type

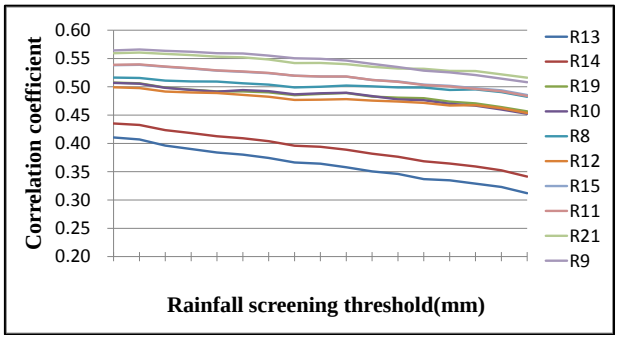

(c) G5(1): slow-descending type

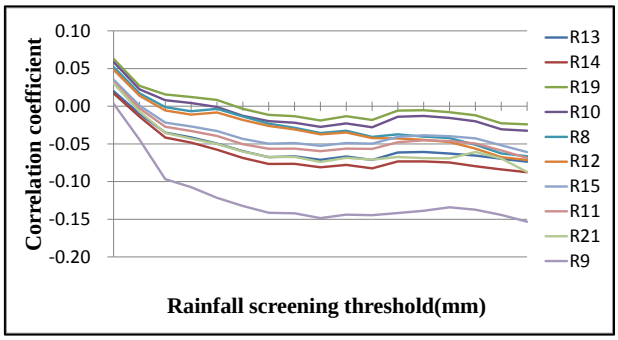

(d) G2: random type

Fig.6. Correlation patterns of groundwater level variations versus rainfall

Table 6 Estimation performance of the BPNN models with different input combinations at four groundwater level monitoring wells

Well【[1]】	Input combination	Corr[2]			RMSE (m)		
		training	validation	testing	training	validation	testing
G1(1)【1, 4, 1 mm, 102.6 m】							
	Streamflow	0.67	0.66	0.66	0.08	0.07	0.10
	Rainfall	0.77	0.76	0.75	0.06	0.08	0.07
	Streamflow*	0.75	0.74	0.71	0.09	0.09	0.11
	Rainfall*	0.81	0.81	0.80	0.08	0.08	0.08
	Rainfall+Streamflow*	0.84	0.83	0.91	0.07	0.07	0.07
G5(1)【1, 3, 0 mm, 78.2 m】							
	Streamflow	0.83	0.83	0.86	0.17	0.15	0.13
	Rainfall	0.81	0.82	0.77	0.16	0.18	0.19
	Streamflow*	0.83	0.84	0.87	0.15	0.19	0.22
	Rainfall*	0.83	0.83	0.81	0.17	0.20	0.17
	Rainfall+Streamflow*	0.88	0.90	0.89	0.15	0.15	0.15
G3【1, 5, 5 mm, 24.1 m】							
	Streamflow	0.38	0.31	0.25	0.12	0.15	0.42
	Rainfall	0.63	0.49	0.43	0.15	0.14	0.22
	Streamflow*	0.59	0.61	0.62	0.13	0.12	0.23
	Rainfall*	0.78	0.78	0.82	0.11	0.18	0.10
	Rainfall+Streamflow*	0.87	0.85	0.82	0.10	0.09	0.12
G4(1)【1, 5, 7 mm, 52 m】							
	Streamflow	0.41	0.31	0.37	0.17	0.30	0.12
	Rainfall	0.44	0.40	0.43	0.19	0.24	0.12
	Streamflow*	0.69	0.65	0.63	0.16	0.13	0.14
	Rainfall*	0.82	0.85	0.82	0.11	0.12	0.12
	Rainfall+Streamflow*	0.89	0.93	0.82	0.08	0.11	0.15

[1]Number of hidden layers, number of neurons, threshold, well depth
[2]Correlation coefficient
*Model with threshold

streamflow has less influence on groundwater level variations. Alternatively, the estimation model combining streamflow and rainfall as inputs has similar performance as the rainfall model with threshold screening in the testing phase (the correlation coefficient is 0.82), which also reveals streamflow has less influence on groundwater level variations.

G4 (1): ladder-type

Similar to G3, the best structure of the BPNN model for G4(1) has one hidden layer and five neurons. Observation data are divided into the training, validation and testing phases in the ratio of 6:2:2, respectively. The total number of groundwater level variation data for G4(1) is 1129. After conducting the rainfall threshold screening at the effective threshold of 7 mm (the 2nd sudden increase in correlation coefficients shown in Fig. 6(b)), only 323 data remain for use. The estimation results indicate that conducting rainfall threshold screening makes excellent improvements in the correlation coefficients for streamflow models (0.37 to 0.63, 70% improvement in the testing phases) and rainfall models (0.43 to 0.82, 91% improvement in the testing phases). In addition, rainfall models outperform streamflow models, which also coincides with the results of G4(1) in Table 5. This might be because G4(1) is located in a distance from the branch of the Jhuoshuei River and the two streamlow gauging stations of the Jhuoshuei River. Alternatively, the estimation model combining streamflow and rainfall as inputs has similar performance as the rainfall model with threshold screening in the testing phase (the correlation coefficient is 0.82), which also reveals streamflow has less influence on groundwater level variations.

In sum, the BPNN can well estimate groundwater level variations, in particular for the models with both streamflow and rainfall as inputs, where the correlation values are all above 0.82 and the RMSE values range from 0.07 to 0.15 m in the testing phases. Groundwater level monitoring wells G1(1), G3(1) and G4(1) are located in a distance from the Zhuoshui river, and therefore they are less affected by the lateral recharge from the river so that rainfall models perform better than strealflow models at these three wells. In contrast, G5(1) is located right next to the Jhuoshuei River, and therefore it is significantly affected by the lateral recharge from the river so that strealflow models perform better than rainfall models at this well.

Conclusion

This study investigates the hydro-system at the mountainous area in the upstream of the Jhuoshuei River basin by using statistic methods and the BPNN based on streamflow, rainfall and daily groundwater level data collected during the periods of 2001 to 2010.

This study first uses the Pearson correlation coefficient to analyze the relationship between groundwater level variation and rainfall as well as streamflow. Several findings are delivered: current groundwater level variation (t) is related to rainfall of the previous day (t-1) while current groundwater level variation (t) is related to current steamflow (t); and the correlation between groundwater level variations versus both shallow and deep groundwater level monitoring wells together with the geologic structures of the wells reveal that the low correlations of the wells (G1(1) and G1(2); G3 and G3(2)) imply clay layers in aquifers can

well separate shallow and deep wells, while the gravel layers in aquifers make the shallow and deep wells (G5(1) and G5(2)) have similar groundwater level variation trends.

The correlations between groundwater level variations and rainfall with threshold screening at for four wells are classified into four types of patterns: slow-ascending type; ladder-type; slow-descending type; and random type. In addition, the depth and geological structure of groundwater level monitoring wells are used to access the causes of those four types. Then, effective rainfall thresholds affecting groundwater level variations are identified: slow-ascending type (G1(1): 1 mm); ladder-type (G3: 7 mm; G4(1): 5 mm); and slow-descending type(G5(1): 0 mm).

This study investigates the groundwater recharge mechanism at mountainous areas by the BPNN for constructing estimation models of groundwater level variations. The results demonstrate that the BPNN models perform rather well because observations and estimations have high correlations and small RMSE values. The groundwater level variations of the groundwater level monitoring well right next to the Jhuoshuei River are significantly influenced by the lateral recharge from the river, and the streamflow model can better estimate than the rainfall model. In contrast, the groundwater level variations of groundwater level monitoring wells far from the Jhuoshuei River are less influenced by the lateral recharge from the river, and the rainfall models can outperform the streamflow models. In addition, estimation models with both rainfall and streamflow as inputs perform the best. With a more understanding about the interactive recharge mechanism between mountainous water resources and groundwater, it can facilitate the discussion on mountainous water resource conservation strategy for alleviating land subsidence in downstream areas, the influence of hydraulic structures on infiltration during rainfall events, and the functions of forests for soil erosion reduction in the future.

Acknowledgements

This study was funded by the Water Resources Agency, Taiwan, ROC (Grant number: MOEAWRA1000439). It is very much appreciated that streamflow and groundwater level data were provided by the Water Resources Agency and rainfall data were provided by the Water Resources Agency, Central Weather Bureau and Taiwan Power Company, Taiwan, ROC.

References

Bredehoeft JD (1967) Response of well-aquifer systems to earth tides. J Geophys Res 72: 3075-3087

Chang LC, Chen PA, Chang FJ (2012) A Reinforced Two-Step-Ahead Weight Adjustment Technique for On-Line Training of Recurrent Neural Networks. IEEE Trans Neural Netw 23(8): 1269-1278

Chang FJ, Kao LS, Kuo YM, Liu CW (2010) Artificial Neural Networks for Estimating Regional Arsenic Concentrations in a Blackfoot Disease Area in Taiwan. J Hydro 388: 65-76.

Chen TS, Jan CD, Chen SH, Tseng CM (2005) Correlation between Groundwater Level Variations and Rainfall Depths. J Taiwan Water Conserv 53(4): 1-12

Chen TS (2006) Study on Rainfall-Induced Groundwater Water Level Variation–Case study at the Naba, Liujar, and Donher Well Stations. Doctoral Dissertation, Department of Hydraulics & Ocean Engineering, National Cheng Kung University, Taiwan, ROC.

Chen YH, Chang FJ (2009) Evolutionary Artificial Neural Networks for Hydrological Systems Forecasting. J Hydro 367:125-137.

Cheng JD, Hong HN, Chou LH (2003) Use Time Series to Analysis Rainfall and Groundwater Level. J Chinese Soil and Water Conserv 35(1):47-56

Daliakopoulos IN, Coulibalya P, Tsanis IK (2005) Groundwater level forecasting using artificial neural networks. J Hydro 1-12.

Jacob C E (1940) The flow of water in an elastic artesian aquifer. Eos Trans. 21: 574-586

Matsumoto N (1992) Regression analysis for anomalous changes of ground water level due to earthquakes. Geophys Res Lett 19(12): 1193-1196

Mamdani EH, Assilian S (1975) Experiment in linguistic synthesis with a fuzzy logic controller. International. J Man-Machine Studies, 7(1): 1-13.

Mendel JM (2001) Uncertain rule-based fuzzy logic systems: introduction and new directions. Prentice-Hall, Inc.

Nourani V, Mogaddam AA, Nadiri AO (2008) An ANN-based model for spatiotemporal groundwater level forecasting. Hydrol Process 22 (26): 5054-5066

Nourani V, Ejlali RG, Alami, MT (2011) Spatiotemporal groundwater level forecasting in coastal aquifers by hybrid artificial neural network-geostatistics model: a case study. Environ EngSci 28 (3): 217-228

Nayak PC, Sudheer KP, Rangan DM, Ramasastri KS (2004) A neuro-fuzzy computing technique for modeling hydrological time series. J Hydro 291(1-2): 52-66

Nayak PC (2006) Groundwater Level Forecasting in a Shallow Aquifer Using Artificial Neural Network Approach. Water ResourManag 20: 77-90

Pearson K (1896) Mathematical contributions to the theory of evolution. III. Regression, heredity and panmixia. Philos. Trans. Royal Soc. London Ser. A 187: 253-318

Rojstaczer S (1988) Determination of fluid flow properties from the response of water levels in wells to barometric loading. Water Resour Res 24(11): 1927-1938

Rumelhart DE, Hinton GE, Williams RJ (1986) Learning internal representations by error propagation, in Rumelhart and McClelland, eds, Parallel Distributed Processing, Vol. I, Foundations, MIT Press, Cambridge, MA, 318-335

Thiessen AH (1911) Precipitation averages for large areas. Monthly Weather Review 39(7): 1082-1084

Van der Kamp G, Gale JE (1983) Theory of earth tides and barometric effects in porous formations with compressible grains. Water Resour Res 19: 538-544

PAWEES 2012 International Conference
Challenges of Water & Environmental Management in Monsoon Asia
27-29 November 2012, Thailand

Estimating Regional Total Phosphate Concentration in a River Basin through the NARX network

Fi-John Chang[1,*], Pin-An Chen[1], Yu-HsuanTsai[1], Ching-Pin Tung[1],Yu-Pin Lin[1], Rita Sau-Wai Yam[1],Li-Chiu Chang[2],Jr-Chuan Huang[3], Shuh-Ji Kao[4],Ta-Wei Chang[5], Wen-Tsun Fang[5]

Abstract Phosphorus is one of the key elements necessary for the growth of plants and animals.Nevertheless, excessive phosphorus has been shown to be a main cause of eutrophication, whichmay lead to large deteriorations in water quality and trophic status.*Total phosphate (TP)* is regarded as an index commonly used in representation of the phosphorus quantity in river water. This study aims to build a model for estimating regional TPconcentrations and recovering missing TP datathrough a dynamical neural architecture of the NARX(Nonlinear Autoregressive with eXogenous input)network. The Dahan Creek located at the downstream of the ShihmenDam is used as a case study. The water quality of the Dahan Creek has decreased rapidly due to heavy pollutant loads from surrounding urban areas.The non-trivial input factors and structures of the NARX network configured with cross-validationare investigated by the Gamma test and Bayesian regularization method, respectively. Results show the proposed NARX network can suitably estimate regional TP concentration and effectively reconstruct the missing TPdata, which can provideuseful information to government decision makers for dealing with river basinmanagement.

KeywordsTotal phosphate (TP), Artificial Intelligence (AI), NARX neural network, Gamma test, Bayesian regularization method, River basinmanagement.

Fi-John Chang(✉) · Ching-Pin Tung · Yu-Pin Lin · RitaSau-Wai Yam
Professor
Dept. of Bioenvironmental Systems Engineering, National Taiwan University, No. 1, Sec. 4, Roosevelt Road, Taipei 10617, Taiwan, ROC.
E-mail: changfj@ntu.edu.tw
Tel: +886-2-33663452; Fax: +886-2-23635854

Li-Chiu Chang
Department of Water Resources and Environmental Engineering, Tamkang University, New Taipei City 25137, Taiwan, ROC
Jr-Chuan Huang
Department of Geography, National Taiwan University, Taipei 10617, Taiwan, ROC
Shuh-Ji Kao
Research Center for Environmental Changes, Academia Sinica, Taipei 11529, Taiwan, ROC
Ta-Wei Chang · Wen-Tsun Fang
Agricultural Engineering Research Center,Taoyuan County32061, Taiwan, ROC

Introduction

The seasonal variation ofsteamflowin Taiwan is very large. In drought seasons, low flows lead to an increase in pollution level. Pollution in the middle and downstreams of rivers is a major environmental issuebecause many industrial facilities and large populated cities are located along them.

Current water quality indexes used in Taiwan are the River Pollution Index (RPI) and Water Quality Index (WQI), designed to assess the conditions of water bodies in rivers, lakes or reservoirs. TheWQI is more sensitive than the RPI and can detect light pollution, especially in the Dahan Creek. Therefore, the WQI is a more suitable index for water quality management.The WQI numerically summarizes the information of multiple water quality parameters into a single value, including Dissolved Oxygen(DO), Coliform Group, pH, Biochemical Oxygen Demand(BOD), Ammonia Nitrite(NH_3-N), Suspended Solid(SS) and Total phosphate(TP). Due to scattered watersheds over Taiwan and high sampling cost, it isunlikely to obtain continuous time series water quality data withcomplete properties at all sampling locations. The WQIcomprises water quality parameters that aresampled monthly, except for the TP that is sampledquarterly.

Total phosphate (TP), a combination of orthophosphate, polyphosphate and organic phosphate, is regarded as an index commonly used in representation of the phosphorus quantity in river water. When phosphorus enters into a river, it is usually in the form of phosphate and is transported from upstream to downstream by flowing water. Orthophosphate chemicals are commonly used in agricultural fertilizers that enter surface water easily during rainfall periods. Polyphosphateis a primary chemical elementadded with considerable amount in the presence of detergents. Organic phosphates are basically formed by biochemical procedures associated with excrement, kitchen waste, water plants, etc. Phosphorus is one of the key elements necessary for the growth of plants and animals. Nevertheless, the anthropogenic nutrient enrichment of natural waters is of environmental importance as it can lead to declines in water quality, changes in biotic population structures and low dissolved oxygen concentrations (Duda, 1993; Carpenter et al., 1998). Excessive phosphorus have been shown to be a main cause of eutrophication, for example, naturally occurring nutrients in large concentrations can often

cause algae blooms (Davis and Koop, 2006; Kristiana et al., 2011).

Artificial neural network (ANN) technology is a computational method inspired by the studies of the brain and nerve systems in biological organisms.In the last decade, ANNs have been widely applied with success to various water resources problems, such as rainfall-runoff modeling (Antar et al., 2006; Chang et al., 2007), flood control (Chang et al., 2008), reservoir operation (Chang et al., 2010; Wang et al., 2010), groundwater problems (Krishna, et al., 2008 ; Nikolos, et al., 2008), and water quality (Chaves and Toshiharu, 2007; McNamara et al., 2008). Recurrent neural networks (RNNs), which belong to a class of ANNs are powerful nonlinear models capable of extracting dynamic behaviors from complex systems through internal recurrence and have attracted much attention for years (Assaad et al., 2005; Chang et al., 2012; Chiang et al., 2010; Ma et al., 2008; Serpen and Xu, 2003). Nonlinear Autoregressive with eXogenous input (NARX) network (Lin et al., 1996) is a subclass of RNNs and is suitable to build the long-term temporal relationship between inputs and outputs(MenezesJr and Barreto, 2008). NARX networks have been demonstrated to be well applied to several nonlinear systems such as waste water treatment plants (Su and McAvoy, 1991; Su et al., 1992) and various time series forecasting (Muhammad and Saeed, 2010). However, its feasibility as a nonlinear tool for time series modeling has not been fully explored yet. Therefore, this study will explore the practical meaning and importance of recurrent connections from the NARX network's output when dealing with regional estimation problems.

In this study, a regional analytical mechanism incorporated with a neural network and several advanced statistical methods is developed and applied to determining the non-trivial factors that control the fluctuations of TP concentrationsas well as building a model for estimating regional TP concentrations. Finally, the reconstructed monthly TP data through a process that adopts the dynamical neural architecture of the NARX network can be analyzed and comprehensively producethe WQI monthlyso that help authorities monitoring hydro-environment much easily and implementing countermeasures in time.

Materials

2.1 Study area

Dahan Creek, one of the most polluted rivers in northern Taiwan. The water quality has decreased rapidly due to heavy pollutant loads from the Taoyuan County, New Taipei City and their surrounding urban areas. The Dahan Creek basin downstream the Shihmen Dam is located at the southwestern end of the New Taipei City and presented in Fig.1. The catchment could be divided conveniently into two zones, based upon land-use morphology. Two zones were designed as the upstream (Shihmen Dam to Yuanshan Weir), downstream (Yuanshan Weir to the confluence point with the Xintian Creek). The upstream sub-catchment presence a better water quality rather than the downstream because of the distinct development level of urbanization.

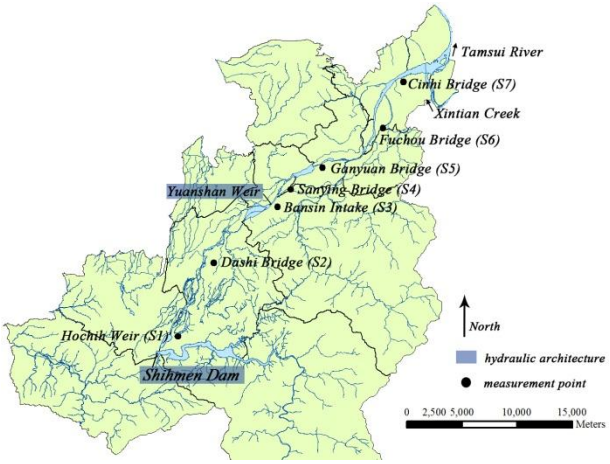

Fig. 1. The Dahan Creek basin downstream the Shihmen Dam and seven water quality gauged stations.

2.2 Data collection

For seven gauged stations on the river channel, a water quality survey was carried out in each month from June 2002 to June 2012. Nine characteristics of the water quality were recorded, including acidity (pH), electro conductivity (EC), dissolved oxygen (DO), biochemical oxygen demand(BOD), chemical oxygen demand (COD), suspended solid (SS), coliform group (Coliform), ammonia nitrogen (NH_3-N) , water temperature (temp). Total phosphate (TP) measurements were also taken at the same place on the river quarterly. And the whole quarterlydata sets are separated into two parts, 2002 to 2009 with 30 length of data in every seven gauged stations are for model calibration purpose, and 2010 to 2012 are used to testing the model.Table 1 shows the statistical analysis of each water quality at whole study area during the period of the model calibration data set, 2002 to 2009, which indicates that the maximum TP concentration have been reached above 6mgl^{-1}. The locations of seven gauged stations are indicated in Fig.1.

A relationship between TP and other water quality variables in the study area are discovered by the correlation coefficient and shown in Fig.2. It can easily find out that EC, BOD, COD, SS, and DO have stronger relationship to TP, with correlation coefficient value higher than 0.5. However, these remarkable variables shown a similar correlation coefficient that presents they may not all trulyaffect fluctuations of TP in our study area, and can hardly determine the prominent ones to reduce the dimension of the model inputs.It clearly indicates that we need more effective method to determine the non-trivial factors from these water quality variables.

Table 1
Water quality of the Dahan Creek during the model calibration period (from 2002 to 2009)

Variable	pH	EC	DO	BOD	COD	SS	Coliform	NH_3-N	temp	TP
		μmho/cm 25℃	mg/L	mg/L	mg/L	mg/L	CFU/100mL	mg/L	℃	mg/L
min	6.6	182	0.00	1.00	4.00	3.6	10	0.02	13.0	0.01
max	10.4	1200	14.10	22.80	535.00	13600	6.8E07	14.40	33.6	6.88
median	8.0	311	7.70	2.60	12.35	38.4	4750	0.36	23.5	0.13
mean	7.9	413	6.70	5.04	23.64	560	858244	1.94	22.9	0.40
SD[1].	0.6	218	3.18	5.20	44.28	1832	5499257	3.12	5.4	0.79
n	210	210	210	210	210	210	210	210	210	210

[1]Standard deviation

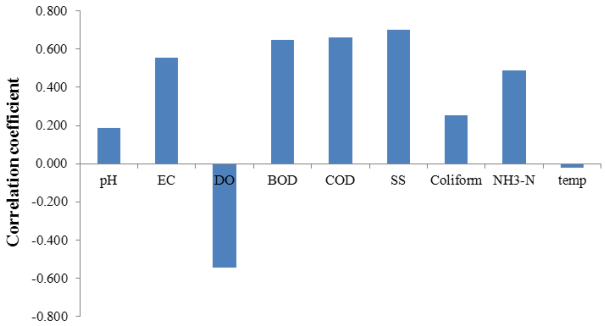

Fig. 2. The relationship between TP and the other water quality parameters (from 2002 to 2009).

Methods

3.1 Gamma test (GT)

The Gamma test(GT),presented byAgalbjorn et al. (1997), can estimate the noise level in a data set and produce estimation directly from the data without assuming anyparametric form of the equations that govern the system. The only requirement is that the system should be governed by a smooth function because the GT will exploit the hypothesized continuity of this governing function.Performing a single Gamma test isa fast procedure, which can provide the noise estimate for each subset of input variables. When the subset for which theassociated noise estimate (Γvalue) is closest to zero, it can be considered as the "best combination" of inputs.Recent applications have noted that the GT combined with ANNs can identify non-trivial input variables effectively (Moghaddamnia et al., 2008; Moghaddamnia et al., 2009; Noori et al., 2011).Therefore, the GT combined with the NARX network is utilized to determine the non-trivial factors that affect thefluctuationof TP concentrationsfrom other nine water quality variables.

3.2 Nonlinear Autoregressive with eXogenous input (NARX) network

NARX is an important class of nonlinear discrete-time systemsthat have two tapped-delay elementsproduced from input and output layers.We focus on the recurrent connection from output-delay terms. Fig.3 shows the architecture of the NARX network. It consists of 3 layers (input, hidden and output layers) and has recurrent connections from the output which may delay several unit times to form new inputs. τ^{-1} is the unit time delay, and $d_Z \geq 1$ is the output-memory order. Therefore, this nonlinear system can be mathematically represented by the following equation:

$$z(t) = f\left[z(t-1),\ldots,z(t-d_z);U(t)\right] \quad (1)$$

where**U**(t) and z(t) denote the input vector and output value of the model at a discrete time step t, respectively. And $f(\cdot)$ is the nonlinear mapping function that needs to be approximated by a learning algorithm.

When the NARX network needs to be trained, it can be one of the following two modes. The first mode is the Series-parallel (SP) mode, where the output's regressor in the input layer is formed only by actual values of the system's output, d(t):

$$z(t) = f\left[d(t-1),\ldots,d(t-d_z);U(t)\right] \quad (2)$$

The other alternative is the Parallel (P) mode, where estimated outputs are fed back into the output's regressor in the input layer and can be mathematically represented as Eq. (6).

It is common that the application of estimating target variables in unrecorded times by a regional model often has poor performance because the information of target variables is not always available in certain gauged stations. Therefore, the NARX network can be trained in the SP mode to construct the relationship between actual and estimated values of target variables. Then the NARX network in the P mode applied to the unrecorded period for improving estimation performance through the recurrent information, ***the estimating values derived from the model***. This is the most import idea of this study that the recurrent connection of the NARX network has practical meaning when dealing with the estimation for the target variable in unrecorded times.

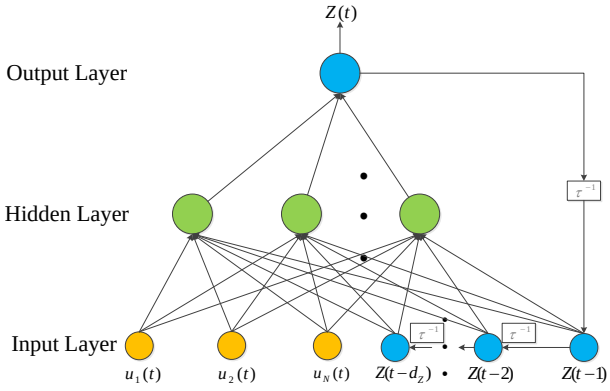

Fig. 3. Architecture of the NARX network without recurrent connection from input-delay terms.

3.3 Bayesian regularization

An appropriate and ideal regional ANN model is the one that produces small errors not only insamples from gauged stations but also in samples from assumed unrecording period. The regularization method proposed by MacKay in 1992 is that an objective function is added to improve the generalization ability of the neural network byconstraining the number and size of network weight values. The idea is based on that the true underlying function is assumed to have a degree ofsmoothnesscontrolled by network parameters, and the network response will be smooth as the parameters keep small. Thus a network is able to sufficiently represent the truefunction, rather than capture the noise.The objective function of the network in the regularization method is given by

$$M(W) = \beta E_D + \alpha E_W \quad (3)$$

whereE_D is the mean square error of network outputs.and$E_W$is a penaltyterm of network complexity in theregularization method. α and β are regularization parameters that can be determined byBayesian techniques.Therefore, the weights ofthe network can be considered as random variables.Let *W*be the network weight vector, *D*be the sampledata, the posterior distribution according to the Bayes' rule is shown as follows:

$$P(W \mid D,\alpha,\beta,\mathrm{H}) = \frac{P(D \mid W,\beta,\mathrm{H})P(W \mid \alpha,\mathrm{H})}{P(D \mid \alpha,\beta,\mathrm{H})} \quad (4)$$

whereP(W|α, H) is the prior density, P(D|W, β, H) is the likelihood function, P(D|α, β, H) is the normalization factor, and H presents the structure of the network. Assuming the noise and the prior distribution forthe weights are both Gaussian, the probability densities can bewritten as:

$$\begin{aligned} P(W \mid D,\alpha,\beta,\mathrm{H}) &= \frac{1}{Z_M(\alpha,\beta)}\exp(-\beta E_D - \alpha E_W) \\ &= \frac{1}{Z_M(\alpha,\beta)}\exp\left[-M(W)\right] \end{aligned} \quad (5)$$

where

$$Z_M(\alpha,\beta) = \int_{-\infty}^{\infty}\left(-M(W)\right)dW \quad (6)$$

From the Bayesian framework, the optimal weights can be derived by maximizing the posterior probability, which is equivalentto minimizing the regularized objective function shown in Eq. (3).

The value of αandβcan also be optimized by applying the Bayes' rule.

$$P(\alpha,\beta \mid D,\mathrm{H}) = \frac{P(D \mid \alpha,\beta,\mathrm{H})P(\alpha,\beta \mid \mathrm{H})}{P(D \mid \mathrm{H})} \quad (7)$$

Therefore, the values ofαandβcan then be inferredat the minimum W_{MP} of *M(W)*,which are shown as:

$$\alpha_{MP} = \frac{\gamma_p}{2E_W(W_{MP})} \quad (8)$$

$$\beta_{MP} = \frac{m-\gamma_p}{2E_D(W_{MP})} \quad (9)$$

where γ_p represents the effective number of network parameters.

3.4 Cross Validation

Cross-validation, which consists of partitioning the data in training and test sets, is commonly used to obtain a reliable estimate of the test error for performance estimation or for use as a model selection criterion. In thek-fold cross-validation for model selection, the first step is to assign a model parameter setting (i.e. initial weights, epoch numbers, number of neurons in the hidden layer, and output-memory orders of the NARX network), and then the original sample is partitioned into k subsamples. Among the k subsamples, a single subsample is retained as validation data for testing the model, and the remaining k-1 subsamples are used as training data. The cross-validation process is then repeated k times, with each of the k subsamples being used exactly once as validation data. The k results from the folds canthen be averaged to produce a single estimation. Therefore, averaged error performances derived from different parameter settings are compared to choose the most appropriate model for further testing the application. k is 42 in this study.

Cross validation can produce a low-bias estimator for the generalization properties of statistical models, and therefore provides a sensible criterion for model selection and performance comparison, especially for samples that are hazardous, costly or impossible to collect, such as the TP concentration in this study.

The proposed regional analytical mechanism is incorporate with four aforementioned advanced statistic methods for dealing with the problem of regional estimation, and its implementation procedure is shown in Fig.4. Therefore, this regional analytical mechanism first effectively extracts non-trivial factors that affect the fluctuations of TP concentrations through the GT. Then the NARX network is utilized to achieve more preciseregional estimation for the TP concentrations of seven stations in the unrecorded time by using the information of the estimated TP concentrations from recurrent connections, and the network complexity is controlled automatically by the Bayesian regularization method to prevent over-fitting. And the cross validation produces a low-bias estimator for the generalization properties of statistical models and provides a sensible criterion for model selection in the calibration stage.

Results and discussion

4.1 Determination of TP-affected water quality factors

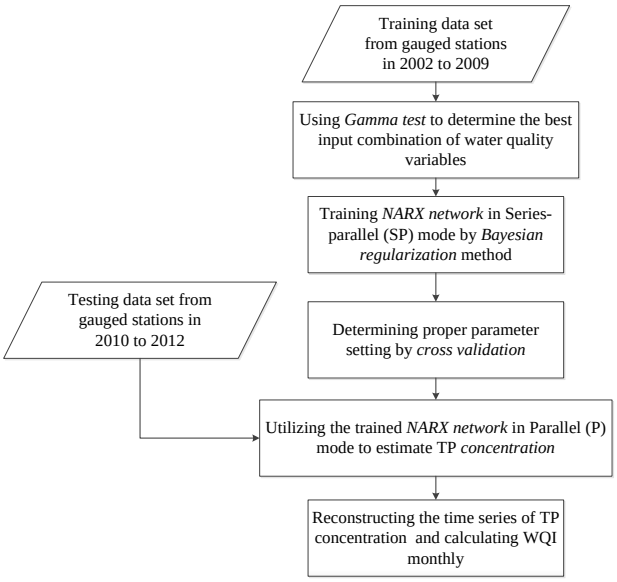

Fig. 4. Procedure of the proposed mechanism for regional analysis

Sufficient data ranging from 2002 to 2009 in seven water quality monitoring stations are first utilized by the GT, and then are used for the calibration of regional estimation models. The data sets of nine water quality factors were scaled to [-1,1] at first, and a total of 2^9-1=511 Γ values corresponding to all possible input combinations can be calculated through the GT. The capability and reliabilityof the GT would increase when analyzing a *set* ofresults. Ifthe frequency ofoccurrence of each input variable in the set ofbest results is examined, we areable to extract only a smallsubset of inputs that are actually relevant to determining the output variable.Therefore, Γ values are sorted in an ascending order. Γvalues smaller than the 10^{th} percentile ($\Gamma_{10} = 0.028$) of all Γ values are defined as the best results of the GT, whereasΓvalues bigger than the 90^{th} percentile ($\Gamma_{90} = 0.217$) of allΓvalues are defined as the worst results of the GT.Fig.5 shows the results of the GT, where the blue bars represent the occurrence frequency of variables in the best results ($F_{\Gamma \le \Gamma_{10}}$)and the red bars represent the occurrence frequency of variables in the worst results ($F_{\Gamma \ge \Gamma_{90}}$).As a result, non-trivial factors affecting fluctuations of TP concentrations are those with higher blue bars and lower red bars simultaneously and can be easily identified by the ratios of$F_{\Gamma \le \Gamma_{10}}toF_{\Gamma \ge \Gamma_{90}}$, shown as the dotted line in Fig.5. The results of the GT demonstrate that EC and SS are non-trivial factors that may significantly affect TP concentrations.The EC has certain relationship with TP concentrations because conductivity in water is affected by the presence of inorganic dissolved solids such as chloride, nitrate, sulfate, phosphate anions or sodium, magnesium, calcium, iron, and aluminum cations (USEPA). Therefore, the rise of TP concentrations in water will result in an increase in conductivity, which depends on the mechanism that hydrolyzes phosphorus in water into the form of phosphate anions.Dissolved inorganic phosphorus interacts strongly with sediments and is involved in various precipitation dissolution reactions, e.g., calcium carbonate phosphate and iron/aluminium oxide minerals (Bowes et al., 2003), which reveals the reason why the SS is also one of the non-trivial factors. It proves that although the GT cannot determine the specific chemicalmechanism, it can still effectively extract non-trivial and meaningful factors that affect the fluctuations of TP concentrations, which are difficult to identify by the traditional correlation matrix shown in Table 1 because the linear correlation cannot be extended to highly non-linear problems.

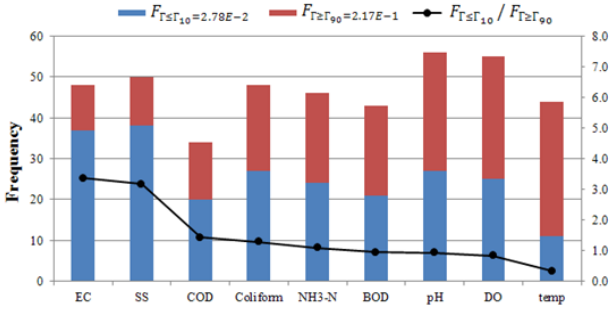

Fig. 5. Determination of non-trivial factors by the GT results.

4.2Regional estimation for TP concentration by the NARX network

Traditional water quality models are either built based on sufficient geological field dataor constructed through the probabilistic theory. However a limited budget on monitoring programs leads to a deficiency of field data. Under this condition, many parameters are estimated by rare data, which may not fit the probabilistic assumption and might cause the difficulty for physical and probabilistic models to estimate certain water quality variables within an acceptable range of errors or uncertainty. Therefore, the NARX network is employedin this study to estimate the regional TP concentration in the Dahan Creek.

Variables EC and SS determined by the GT in seven gauged stations are used as exogenous inputs to the NARX network. The data sets in seven gauged stations monitored between 2002 and 2009 are used for model calibration.Therefore, the NARX network in the SP mode trained by the Bayesian regularization method is calibrated by a 42-fold cross validation.The most appropriate NARX network comprises two inputs of water quality variables, two output-memory orders and 10 hidden layer neurons, and the effective number of the trained network parameters, γ_p, is 37.74. To explore the effective and useful NARX network in the regional estimation task, the backpropagation neural network (BPNN) that represents a classical type of ANNs is also implemented with a similar network structure (without recurrent connections) to the NARX network.The

BPNN trained with the Levenberg-Marquardt optimizationalgorithm is also calibrated by a 42-fold cross validation.The constructed BPNN consists of two inputs of water quality variables(the same as those of the NARX network) and six hidden layer neurons. The results show the average root mean square error (RMSE) of the NARX network in the training and validation phases are 0.188 and 0.375mgl^{-1}, respectively, whereas the average RMSE of the BPNN in the training and validation phases are significantly increased to 0.262 and 0.665mgl^{-1}, respectively. It is worth noting that the effective number of network parameters, γ_p, has been optimized from the original 61 to 37.74 after the calibration of the NARX network. This demonstrates that the Bayesian regularization method can effectively control the number of network parameters that are well determined by the data and can equivalently reduce the network size to avoid the over-fitting problem caused in a rather complex network structure. As a result, the NARX network derives acceptable resultswhen comparing the mean and standard deviation (0.40±0.79mgl^{-1}) of the TP concentrations in seven gauged stations and has similar performance in the training and validation phases while the BPNN requires fewer hidden layer neurons to prevent the over-fitting problem but still performs poorly in the validation phase.

After finishing the model calibration, the observed TP concentrations in seven gauged stationsfrom2010 to 2012 are utilized to test the two constructed regional models, and the TP concentration data collected during March and June in 2010are used as the initial values of the output regressor in the NARX network in the P mode. In addition to RMSE, mean absolute error (MAE), Nash–Sutcliffe model efficiency coefficient (E),and the correlation coefficient (CC) are also used in the testing stage for comparison purpose. E is defined as:

$$E = 1 - \frac{\sum_{i=1}^{n}(O_i - \hat{Z}_i)^2}{\sum_{i=1}^{n}(O_i - \overline{O})^2} \quad (10)$$

where O_i is the observed TP concentration during the i^{th}recorded time of the same year in seven gauged stations, $\hat{Z}_i$ is the estimated TP concentration during the i^{th}recorded time of the same year in seven gauged stations, $\overline{O}$ represents the average of the observed TP concentrations of seven gauged stations in a certain year, and n is the length of data.

The result of model comparison is summarized in Table 2. The results indicate that the NARX network has smaller RMSE and MAE values but much higher E and CC values than the BPNN. The serial estimations of the TP concentrations in seven gauged stations in three different testing years obtained from the NARX network and BPNN are shown in Fig.6. It indicates that although the NARX network has some underestimation in the high TP concentration, it can still well extract the trend of the TP concentrations in seven gauged stations in all three different years, whereas the BPNN can not reflect the fluctuation of the TP concentrations in most gauged stations. The BPNN even produces a reverse trend when being compared with observed TP concentrations time series, especially in the downstream gauged stations with higher TP concentrations. Fig.7 shows the scatter plots of observed and estimated TP concentrations for 2010 up to 2012, which are derived from the NARX network and the BPNN. The estimation values derived from the NARX network are close to the ideal line and only have some underestimated points at high values. However the BPNN has poor estimation ability when the TP concentration is higher than 0.2 mgl^{-1}.Therefore, the NARX network can adequately utilize the information of model outputs through recurrently connecting to the network itself. The NARX network coupled with the Bayesian regularization methodshows an impressive generalizability and derives reliable estimation of regional TP concentrations when comparing the mean and standard deviation of the TP concentrations in the whole gauged stations in three different testing years and four aforementioned performance criteria.

4.3Reconstructing the time series of TP concentration and calculating WQI

From the previous section, the NARX network can provide reliable point estimation and extract the trend of TP concentration in seven gauged stations. Therefore, it can be utilized to reconstruct the time series of TP concentrations from quarterly to monthly monitoring scale. Figure 8 shows the reconstructed monthly time series and quarterlymonitoredtime series of the TP concentrations in seven gauged stations from 2010 to2012. It reveals that the TP concentrations in two gauged stations (S6 and S7) which located relatively close to the downstream, have intensive oscillation inalmost every month, which cannot be easily detected based only on quarterly data. Moreover, the monthly WQI can then be calculated (Fig.9). It also indicates that the WQI scores are at the level of either bad or poor water quality in S6 and S7 in almost every month. Such clear and powerful information can be provided to the government for making more management effortsin these two gauged stations and their surrounding areas.

Conclusion

In this study, a regional analytical mechanism incorporated mainly with a neural network and four advanced statistical methods is developed and applied to the estimation of TP concentrations in the Dahan Creek. It is difficult to identify non-trivialfactors by traditional correlation matrix because of the highly nonlinearity or unknown complex mechanisms in certain parts of the study area. Therefore, the GT is first used to effectively extract non-trivial and meaningful factors (EC and SS variables) from a large number of possible input

Table 2
Performance of the NARX network and the BPNN for TP concentration estimation in seven gauged stations from 2010 to 2012

		RMSE (mgl^{-1})	MAE (mgl^{-1})	E	CC	Mean (mgl^{-1})	SD[1]. (mgl^{-1})
NARX network	Estimation in 2010	0.075	0.052	0.86	0.95	0.222	0.210
	Estimation in 2011	0.151	0.102	0.73	0.92	0.237	0.297
	Estimation in 2012	0.057	0.037	0.79	0.90	0.147	0.130
BPNN	Estimation in 2010	0.230	0.144	-0.30	0.25	0.222	0.210
	Estimation in 2011	0.276	0.181	0.11	0.40	0.237	0.297
	Estimation in 2012	0.136	0.102	-0.18	0.25	0.147	0.130

[1]Standard deviation

(a)

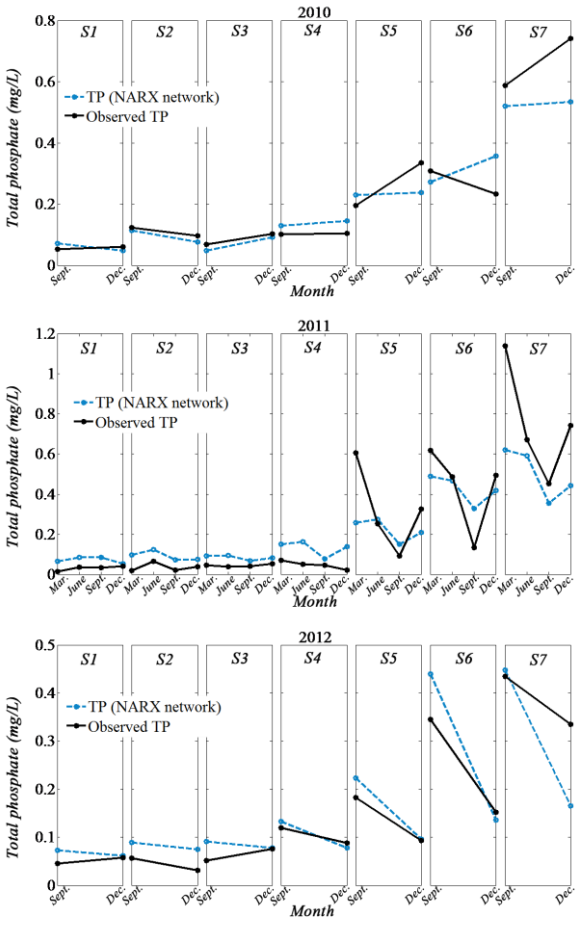

(b)

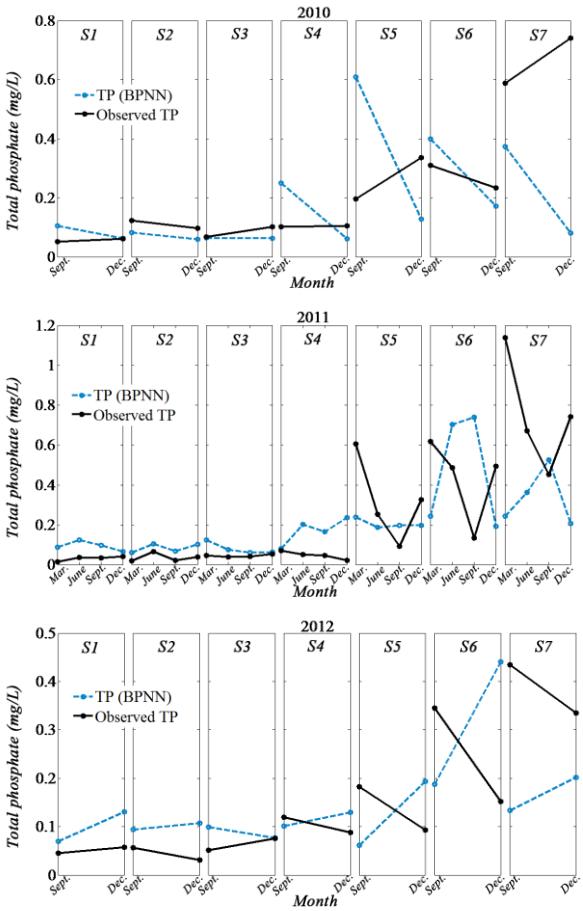

Fig.6. Serial estimation of the TP concentrations in seven gauged stations in three different testing years by (a) NARX network and (b) BPNN

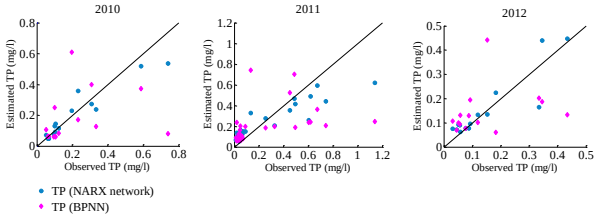

Fig.7. Scatter plots of observed and estimatedTP concentrations derived from the NARX network and the BPNN in seven gauged stations from 2010 to 2012.

combinations that affect the target variable (TP concentration). Then the NARX network trained by the Bayesian regularization method adequately utilizes the information of model outputs through recurrent connections to the network itself for estimating the target variable at unrecorded period, which solves the over-fitting problem and improves the generalization ability of network models. Besides, cross validation can produce a low-bias estimator of the generalization properties of network models and provide a sensible criterion for model selection and performance comparison in the calibration stage of network models. In the calibration and testing stages, the NARX network

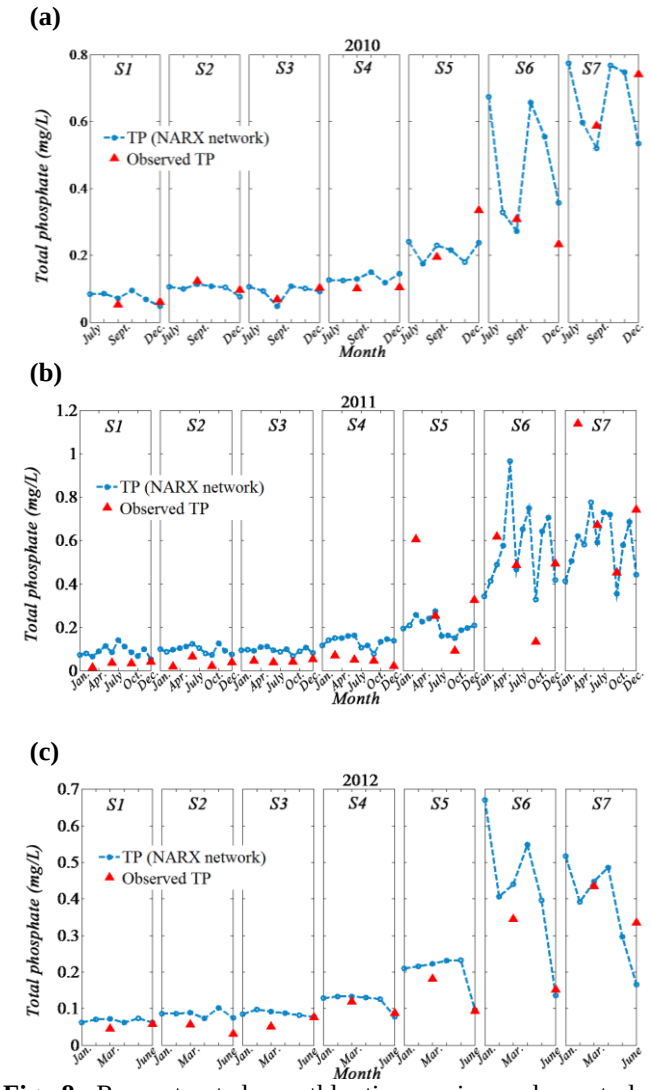

Fig. 8. Reconstructed monthly time series and quarterly monitored time series of the TP concentrations in seven gauged stations from (a) 2010 to (c) 2012.

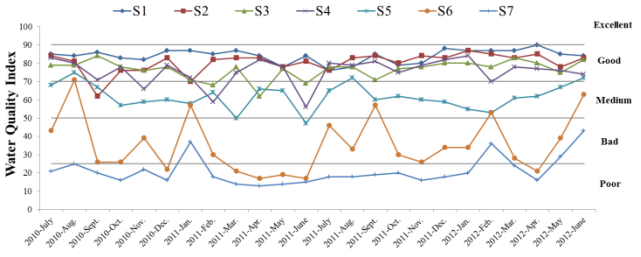

Fig. 9. Reconstructed monthly WQI in seven gauged stations from 2010 to 2012.

has much better performance than the BPNN, which proves the importance of the information of model outputs in the problem of regional estimation. Finally, the constructed NARX network can be utilized to reconstruct the time series of TP concentrations from quarterly to monthly monitoring scale, which is meaningful and helpful for the government to make more efforts on those gauged stations and their neighborhood that have intensive oscillation of TP concentrations. We believe that the proposed regional analytical mechanism can be easily and appropriately applied to regional estimation problems for estimating missing, hazardous or costly data in other study areas, which needs to be further explored in our future works.

Acknowledgements

This study was partially funded by the National Science Council, Taiwan, ROC (Grant numbers: 101-2923-B-002-001-MY3, 100-2313-B-002-011-MY3). It is very much appreciated that water quality data were provided by the Environmental Protection Administration, Taiwan, ROC.

References

Agalbjorn S, Koncar N, Jones A.J.(1997) A note on the gamma test, Neural Comput. Appl., 5 131-133

AntarM.A., Elassiouti I, Allam M.N.(2006) Rainfall-runoff modelling using artificial neural networks technique: a Blue Nile catchment case study, Hydrological Processes 20,1201-1216.

Assaad M, Boné R, Cardot H (2005) Study of the Behavior of a New Boosting Algorithm for Recurrent Neural Networks Artificial Neural Networks: Formal Models and Their Applications - ICANN 2005, Lecture Notes in Computer Science:169-174

Ardalani-Farsa M,Zolfaghari S. (2010) Chaotic time series prediction with residual analysis method using hybrid Elman-NARX neural networks. Neurocomput. 73(13-15), 2540-2553

Bowes M.J., House W.A., Hodgkinson R.A. (2003)Phosphorus dynamics along a rivercontinuum.The Science of the Total Environment 313 , 199-212.

Carpenter SR, Caraco NF, Correll DL, Howarth RW, Sharpley AN, Smith VH. (1998) Nonpoint pollution of surface waters with phosphorus and nitrogen.EcolAppl8(3):559-568

Chang L.C., Chang, F.J., Hsu H.C.(2010)Real-Time Reservoir Operation for Flood Control Using Artificial Intelligent Techniques. International Journal of Nonlinear Sciences and Numerical Simulation 11(11), 887-902

Chang L.C., Chen P.A., Chang F.J. (2012) A Reinforced Two-Step-Ahead Weight Adjustment Technique for On-Line Training of Recurrent Neural

Networks.IEEE Trans Neural Networkand Learning Systems23(8): 1269-1278

Chang, F.J., Chang, K.Y., Chang, L.C.(2008)Counterpropagation fuzzy-neural network for city flood control system. Journal of Hydrology 358, 24-34.

Chang, F.J., Chiang, Y.M., Chang, L.C.(2007) Multi-step-ahead neural networks for flood forecasting. Hydrological Sciences Journal 52(1), 114-130.

Chang, L.C., Chang, F.J. (2001)Intelligent control for modeling of real time reservoir operation. Hydrological Processes 15(9), 1621-1634.

Chaves, P, Toshiharu, K(2007) Conceptual fuzzy neural network model for water quality simulation. Hydrological Processes 21(5), 634-646.

Chiang Y.M., Chang L.C., Tsai M.J., Wang Y.F., Chang F.J., (2010) Dynamic Neural Networks for Real-Time Water Level Predictions of Sewerage Systems-covering gauged and unguaged sites, Hydrol. Earth Syst. Sci. 14, 1309-1319

Davis, J, Koop, K(2006) Eutrophication in australian rivers, reservoirs and520 estuariesa southern hemisphere perspective on the science and its implica-tions. Hydrobiologia 559 (1), 23-76

Duda AM. (1993) Addressing nonpoint sources of water-pollution must become an international priority.WaterSciTechnol28(3–5):1-11

Krishna B, Rao Y.R.S., Vijaya T(2008)Modelling groundwater levels in an urban coastal aquifer using artificial neural networks. Hydrological Processes 22, 1180-1188.

Kristiana R, Vilhena L, BeggG, Antenucci J, Imberger J(2011) The management of lake burragorang in a changing climate: The application of the index of sustainable functionality. Lake and Reservoir Management 27 (1),70-86

Lin T, Horne B.G., Tino P, Giles C.L.(1996)Learning long-term dependencies inNARX recurrent neural networks. IEEE Trans., Neural Networks 7 (6) ,1424-1438

Ma Q.L., Zheng Q.L., Peng, H,Zhong T.W., Qin, J.W. (2008) Multi-step-prediction of chaotic time series based on co-evolutionary recurrent neural network. Chinese Physics B 17(2), 536

MacKay D.J.C. (1992) Bayesian interpolation. Neural Comput 4, 415–447

McNamara, J.P., Kane, D.L., Hobbie, J.E., Kling, G.W.(2008) Hydrologic and biogeochemical controls on the spatial and temporal patterns of nitrogen and phosphorus in the Kuparuk River arctic Alaska. Hydrological Processes 22, 3294-3309.

MenezesJr J.M.P.,Barreto G.A.(2008) Long-term time series prediction with the NARX network: An empirical evaluation.Neurocomputing 71(16-18), 3335-3343

Moghaddamnia A, Ghafari M, Piri J, Amin S, Han D (2009) Evaporation estimation using artificial neural networks and adaptive neuro-fuzzy inference system techniques. Advances in Water Resources32, 88-97

Moghaddamnia A,Ghafari M, Piri J,Han D(2008) Evaporation estimation using support vector machines technique. World Academy of Science, Egineering and Technology43, 14-22

Nikolos, I.K., Stergiadi, M., Papadopoulou, M.P., Karatzas, G.P.(2008) Artificial neural networks as an alternative approach to groundwater numerical modelling and environmental design. Hydrological Processes22,3337-3348

Noori R, Karbassi AR, Moghaddamnia A, Han D, Zokaei-Ashtiani M.H., Farokhnia A, Gousheh M.G. (2011) Assessment of input variables determination on the SVM model performance using PCA, Gamma test, and forward selection techniques for monthly stream flow prediction. Journal of Hydrology401, 177-189

Serpen G, Xu Y (2003) Simultaneous recurrent neural network trained with non-recurrent backpropagation algorithm for static optimisation. Neural Computing & Applications 12: 1-9. DOI 10.1007/s00521-003-0365-0

Su H.T.,McAvoy T.J.(1991) Identification of chemical processes usingrecurrent networks, in Proc. Amer. Contr. Conf. 3, 2314-2319

Su H.T., McAvoy T.J., Werbos P(1992) Long-term predictions ofchemical processes using recurrent neural networks: A parallel trainingapproach. Ind. Eng. Chem. Res. 31, 1338-1352

WangY.M., Chang J.X., Huang Q(2010) Simulation with RBF Neural Network Model for Reservoir Operation Rules. Water Resources Management 24(11), 2597-2610.